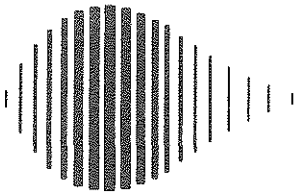

NATIONAL CENTER FOR EARTHQUAKE
ENGINEERING RESEARCH
State University of New York at Buffalo

EXPERIMENTAL EVALUATION OF INSTANTANEOUS OPTIMAL ALGORITHMS FOR STRUCTURAL CONTROL

by

R.C. Lin, T.T. Soong and A.M. Reinhorn
Department of Civil Engineering
State University of New York at Buffalo
Buffalo, NY 14260

Technical Report NCEER-87-0002

April 20, 1987

This research was conducted at the State University of New York at Buffalo and was partially supported by the National Science Foundation under Grant No. ECE 86-07591.

NOTICE

This report was prepared by State University of New York at Buffalo as a result of research sponsored by the National Center for Earthquake Engineering Research (NCEER). Neither NCEER, associates of NCEER, its sponsors, State University of New York at Buffalo, nor any person acting on their behalf:

a. makes any warranty, express or implied, with respect to the use of any information, apparatus, method, or process disclosed in this report or that such use may not infringe upon privately owned rights; or

b. assumes any liabilities of whatsoever kind with respect to the use of, or for damages resulting from the use of, any information, apparatus, method or process disclosed in this report.

EXPERIMENTAL EVALUATION OF INSTANTANEOUS OPTIMAL ALGORITHMS FOR STRUCTURAL CONTROL

by

R.C. Lin[1], T.T. Soong[2], and A.M. Reinhorn[3]

April 20, 1987

Technical Report NCEER-87-0002

NCEER Contract Number 86-3021

NSF Master Contract Number ECE 86-07591

and

NSF Grant No. CEE 8311879

1 Graduate Research Assistant, Department of Civil Engineering, State University of New York at Buffalo
2 Professor, Department of Civil Engineering, State University of New York at Buffalo
3 Associate Professor, Department of Civil Engineering, State University of New York at Buffalo

NATIONAL CENTER FOR EARTHQUAKE ENGINEERING RESEARCH
State University of New York at Buffalo
Red Jacket Quadrangle, Buffalo, New York 14261

ABSTRACT

In a continuing effort to determine the feasibility of applying optimal control to building structures, a comprehensive experimental study was carried out using a standardized structural model under base excitation supplied by the Seismic Simulator at SUNY/Buffalo. Based upon computer simulated and experimental results, this report presents a comparison of efficiencies of several optimal control algorithms using instantaneous optimal criteria, including time delay compensation. All investigations were done under similar conditions to permit a systematic evaluation of efficiency. Comparisons were also made between analytical and experimental results and between instantaneous control algorithms and classical closed-loop linear feedback. Conclusions are drawn regarding relative merits of control algorithms considered under varying conditions.

TABLE OF CONTENTS

LIST OF ILLUSTRATIONS

LIST OF ILLUSTRATIONS (CONT'D)

LIST OF ILLUSTRATIONS (CONT'D)

LIST OF TABLES

SECTION 1
INTRODUCTION

To study active control applied to structures subjected to various types of dynamic loads, many control algorithms have been developed. One of them is the closed-loop optimal control with classical quadratic performance index (also called 'global optimal control'). For a single-degree-of-freedom system, the performance index [ref. 1] is

$$J = \int_0^{t_f} (kx^2(t) + \beta k_c u_c^2(t))\, dt \qquad (1)$$

where:

$x(t)$ = Displacement relative to the base
$u_c(t)$ = Displacement of the actuator
k = Structural stiffness
k_c = Stiffness of the tension cable
t_f = Duration defined to be longer than that of the base excitation
β = Weighting factor

The feasibility of using this control algorithm has been verified experimentally [ref. 1], but apparently cannot be used for open-loop or open-closed-loop control. In open-loop control or open-closed-loop control, the excitation should be regarded as a feedback value introduced into the control algorithms. Thus, using classical optimal control, the excitation history applied to the structures should be known a priori so that the Riccati matrix can be solved. Therefore, the classical open-loop or open-closed-loop control cannot be used if excitations are random such as those due to earthquakes.

In considering the seismic excitation, although the entire earthquake history shaking the base of the structure is not known a priori, it can be measured in real-time using sensors attached to the structure. In other words, at any time t, the earthquake record is available up to that time instant t. Such measured information can be used to develop new optimal control algorithms [ref. 2]. This can be accomplished by, for example, choosing an objective function which takes the form of a time-dependent performance index in terms of the quadratic funtions as

$$J(t) = \underset{\sim}{z}^T(t)\, Q\, \underset{\sim}{z}(t) + \underset{\sim}{u}^T(t)\, R\, \underset{\sim}{u}(t) \qquad (2)$$

where:

$\underset{\sim}{z}(t)$ = State vector
$\underset{\sim}{u}(t)$ = Control force vector
Q and R = Weighting matrices

The quadratic performance index is minimized at every time instant, referred to as the 'instantaneous optimal control.' These control algorithms, including instantaneous optimal open-loop control, open-closed-loop control and closed-loop control have been developed in [ref. 2].

In this study, an experimental investigation was made using the instantaneous optimal control algorithms to evaluate their feasibility. Experiments were carried out on a model structure modeling a single-degree-of-freedom system. Comparisons are made between analytical and experimental results and between instantaneous control algorithms and classical closed-loop linear feedback.

SECTION 2
EXPERIMENTAL SET-UP AND MODEL STRUCTURE

The experiments were carried out on a 12 ft. by 12 ft. shaking table which can simulate various excitations including seismic excitations. The table has five degrees of freedom, of which three (vertical, lateral and roll) can be individually programmed. The capacity of the table allows shaking of a structural model's weighting up to 50 metric tons (110 kip) with a maximum acceleration of 0.55g. A more detailed description of the shaking table can be found in [ref. 3].

The model structure is a three-story steel frame modeling a shear building by the method of artificial mass simulation. In this study, the top two floors of the model were rigidly braced to behave as a single-degree-of-freedom system. Figure 2-1 shows its configuration in the laboratory. Some of its properties are as follows: mass (m) = 16.7 lb-sec.^{2}/in (2921 kg), height = 8'-4" (2.53 m), natural frequency (ω) = 3.52 Hz, stiffness of structure (k) = 8169 lb/in (1431 kN/m), and damping factor (ζ) = 1.25%.

The control forces were supplied by a servo controlled hydraulic actuator through a system of tendons attached to the structure as shown in Figure 2-2. The tendons were pretensioned to about 500 lb. (2.23 kN), approximately half of their strength, to insure that they were under tension at all times. The stiffness of the tendons was 2312.6 lb/in (405 kN/m) and their angle of inclination was 36.4° from the horizontal.

The model structure was bolted to a concrete block which in turn was bolted to the center of the shaking table, which supplies the desired base excitation. State variable measurements were made by means of strain gage bridges installed on the columns just below the first-floor slab. The signal from one strain gage bridge was used as the measured relative displacement signal while the signal from the second was further passed through an analog differentiator and was regarded as the measured relative velocity. The base acceleration was directly measured by an accelerometer installed on the concrete block at the basis of the structure. The sensing and control system is shown in the block diagram in Figure 2-3.

The data acquisition system to monitor the experimental results consisted of a high-speed PDP 11/34 digital computer with analog-digital converters and 52 channels of conditioning, amplification and low-frequency filters. A spectrum analyzer was used to give frequency domain response function which was subsequently recorded.

More detailed description of the experimental facilities can be found in [refs. 3, 4].

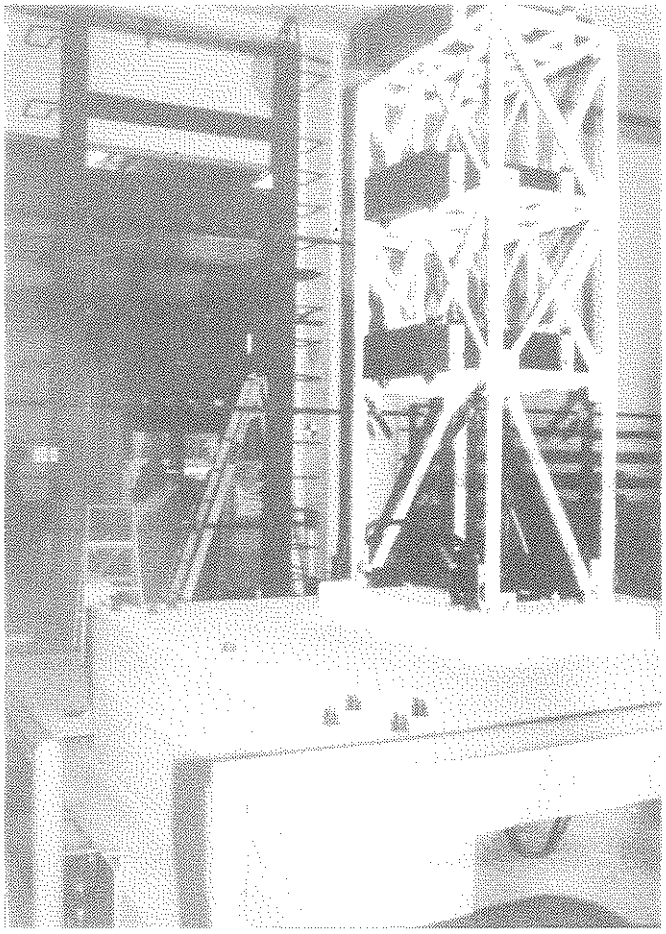

FIGURE 2-1 View of Model and Test Set-Up

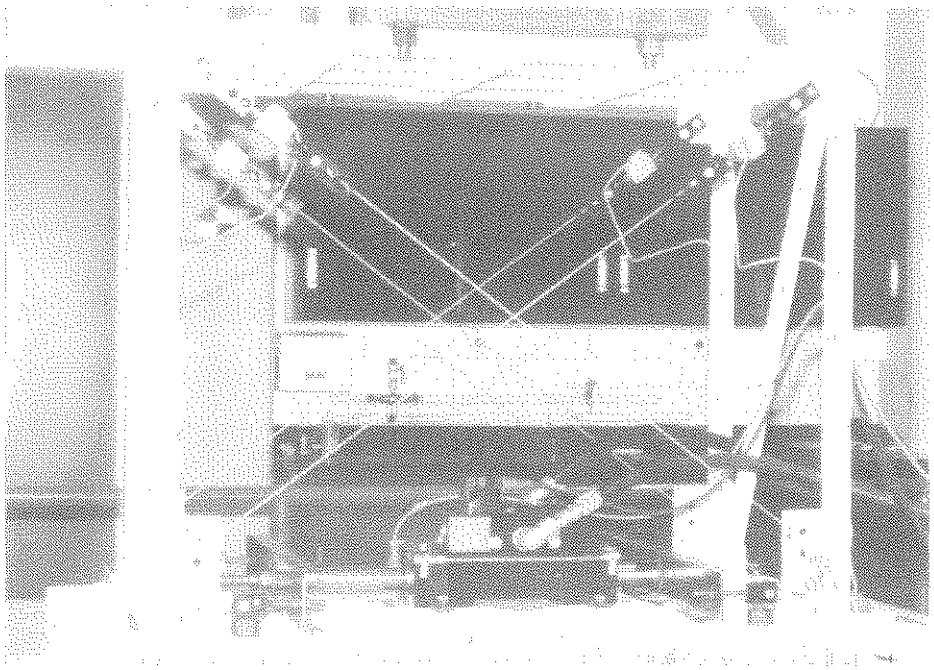

FIGURE 2-2 View of Tendons and Hydraulic Actuator

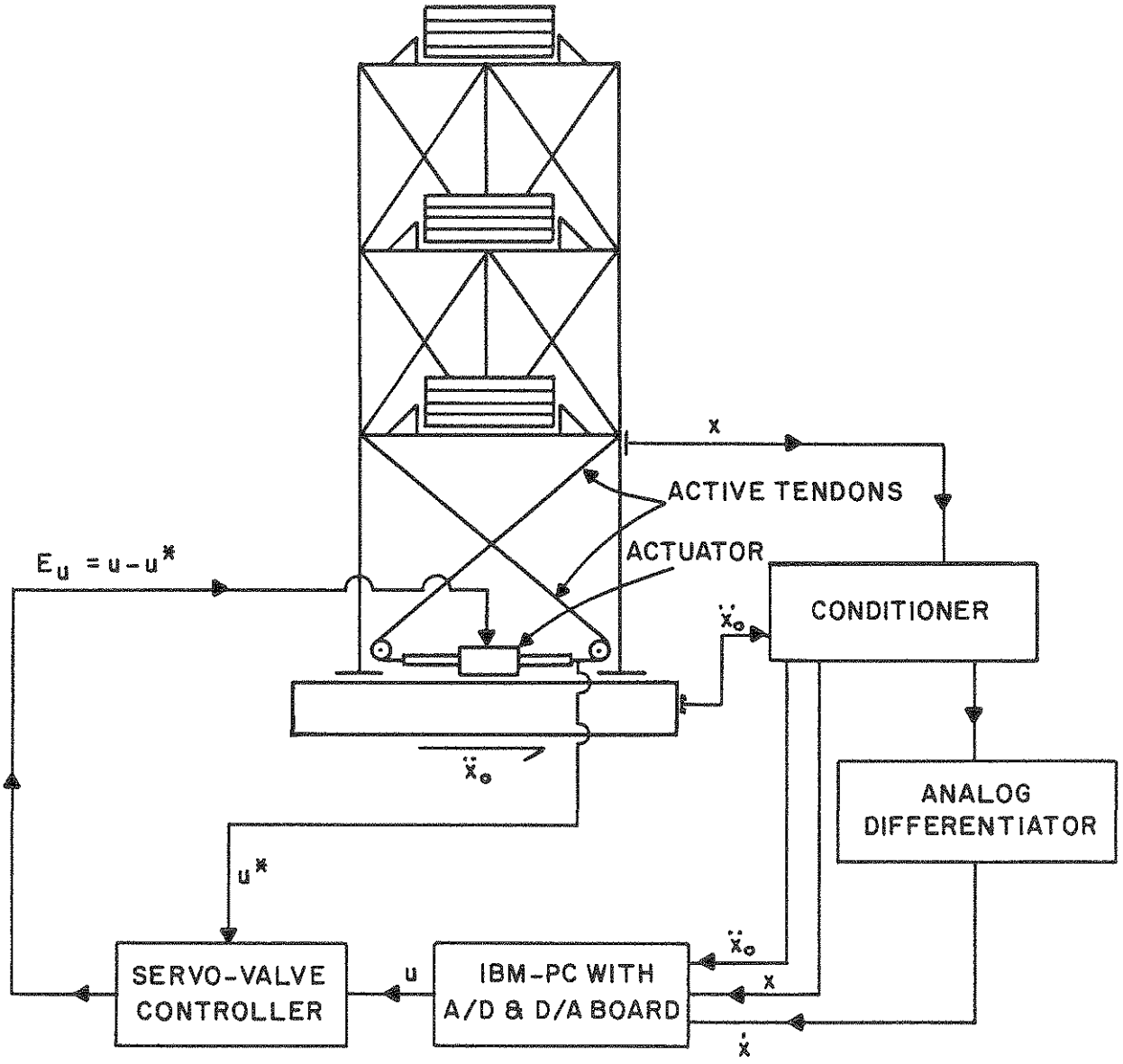

FIGURE 2-3 Block Diagram of Control System

SECTION 3
CONTROL ALGORITHMS

3.1 Numerical Solution of Equations of Motion

A shear building can be modeled as a multi-degree-of-freedom system. The equations of motion can be expressed by the matrix equation

$$M \ddot{\underset{\sim}{x}}(t) + C \dot{\underset{\sim}{x}}(t) + K \underset{\sim}{x}(t) = - M \ddot{\underset{\sim}{x}}_O(t) + B_1 \underset{\sim}{u}(t) \tag{3}$$

where:

$\underset{\sim}{x}(t)$ = Displacement vector relative to the base
$\ddot{\underset{\sim}{x}}_O(t)$ = Excitation vector
$\underset{\sim}{u}(t)$ = Control force vector
B_1 = Control force location matrix
M = System mass matrix
C = Damping matrix
K = Stiffness matrix

Equation (3) can be rewritten in the state-space form

$$\dot{\underset{\sim}{z}}(t) = A \underset{\sim}{z}(t) + B \underset{\sim}{u}(t) + W_1 \ddot{\underset{\sim}{x}}_O(t) \tag{4}$$

The state equation given in Eq. (4) can be decoupled using the transformation

$$\underset{\sim}{z}(t) = T \underset{\sim}{y}(t) \tag{5}$$

where:

T = Modal matrix whose columns are the eigenvector of A
$\underset{\sim}{y}(t)$ = Generalized state vector

Upon substituting Eq. (5) into Eq. (4), one obtains the decoupled equation of motion

$$\dot{\underset{\sim}{y}}(t) = \Theta \underset{\sim}{y}(t) + \underset{\sim}{f}(t) \; ; \; \underset{\sim}{y}(0) = 0 \tag{6}$$

where:

$\Theta = T^{-1} A T$
$\underset{\sim}{f}(t) = T^{-1} B \underset{\sim}{u}(t) + T^{-1} W_1 \ddot{\underset{\sim}{x}}_O(t)$ (7)

The solution of Eq. (6) can be written as

$$\underset{\sim}{y}(t) = \int_0^t \exp[\Theta\,(t-\tau)]\,\underset{\sim}{f}(\tau)\,d\tau \tag{8}$$

The solution for the generalized response vector given by Eq. (8) can be obtained numerically using the trapezoidal rule, i.e.

$$\underset{\sim}{y}(t) = \sum_{k=1}^{n-1} \exp[\Theta\,(n-k)\,\Delta t]\,\underset{\sim}{f}(k\Delta t)\,\Delta t + \underset{\sim}{f}(t)\,(\Delta t/2) \tag{9}$$

where:

Δt = Computation time interval.

For simplicity, let

$$\underset{\sim}{d}(t-\Delta t) = \sum_{k=1}^{n-1} \exp[\Theta\,(n-k)\,\Delta t]\,\underset{\sim}{f}(k\Delta t)\,\Delta t \tag{10}$$

such that Eq. (9) can be expressed as

$$\underset{\sim}{y}(t) = \underset{\sim}{d}(t-\Delta t) + \underset{\sim}{f}(t)\,(\Delta t/2) \tag{11}$$

Substituting Eq. (11) into Eq. (5) leads to

$$\underset{\sim}{z}(t) = T\,[\underset{\sim}{d}\,(t-\Delta t) + \underset{\sim}{f}(t)\,(\Delta t/2)] \tag{12}$$

Using step-by-step computation, the vector $\underset{\sim}{d}(t)$ can be expressed as

$$\underset{\sim}{d}(t) = \exp(\Theta\Delta t)\,[\underset{\sim}{d}\,(t-\Delta t) + \underset{\sim}{f}(t)\,\Delta t] \tag{13}$$

The vector $\underset{\sim}{d}(t)$ can be obtained from the measured state vector.

Substituting Eq. (12) into Eq. (13), one gets

$$\underset{\sim}{d}(t) = \exp(\Theta\Delta t)\,[T^{-1}\,\underset{\sim}{z}(t) + \underset{\sim}{f}(t)\,(\Delta t/2)] \tag{14}$$

or

$$\underset{\sim}{d}(t-\Delta t) = \exp(\Theta\Delta t)\,T^{-1}\left[\underset{\sim}{z}(t-\Delta t) + \frac{\Delta t}{2}\,(B\,\underset{\sim}{u}\,(t-\Delta t) + W_1\ddot{\underset{\sim}{x}}_o\,(t-\Delta t))\right] \tag{15}$$

For a single-degree-of-freedom system, the equation of motion can be expressed as

$$\ddot{x}(t) + 2\zeta\omega\dot{x}(t) + \omega^2 x(t) = -\ddot{x}_o(t) + \frac{1}{m}u(t) \tag{16}$$

The state equation is

$$\dot{\underset{\sim}{z}}(t) = A\,\underset{\sim}{z}(t) + B\,u(t) + W_1\,\ddot{x}_o(t) \tag{17}$$

in which $\underset{\sim}{z}(t) = \begin{bmatrix} x(t) \\ \dot{x}(t) \end{bmatrix}$; $A = \begin{bmatrix} 0 & 1 \\ -\omega^2 & -2\zeta\omega \end{bmatrix}$; $B = \begin{bmatrix} 0 \\ \frac{1}{m} \end{bmatrix}$; $W_1 = \begin{bmatrix} 0 \\ -1 \end{bmatrix}$

where:
m = Mass
ω = Natural frequency
ζ = Damping factor

These dynamic parameters of structure can be obtained from system identification tests [ref. 3].

Following Eqs. (12) and (13), the solution of Eq. (17) has the form

$$\underset{\sim}{z}(t) = T\left[\underset{\sim}{d}(t-\Delta t) + \underset{\sim}{f}(t)\,(\Delta t/2)\right]$$

$$= T\left[\underset{\sim}{d}(t-\Delta t) + \frac{\Delta t}{2}T^{-1}(B\,u(t) + W_1\,\underset{\sim}{x}_o(t))\right] \tag{18}$$

and

$$\underset{\sim}{d}(t) = \exp(\Theta\,\Delta t)\left[\underset{\sim}{d}(t-\Delta t) + T^{-1}(B\,u(t) + W_1\,\underset{\sim}{x}_o(t))\,\Delta t\right] \tag{19}$$

where

$$T = \begin{bmatrix} 1 & 1 \\ -(\zeta\omega+\omega_d) & -(\zeta\omega-\omega_d) \end{bmatrix}; \quad T^{-1} = \begin{bmatrix} -\frac{\zeta\omega-\omega_d}{2\omega_d} & \frac{-1}{2\omega_d} \\ \frac{\zeta\omega+\omega_d}{2\omega_d} & \frac{1}{2\omega_d} \end{bmatrix}$$

$$\omega_d = \omega \sqrt{1 - \zeta^2}$$

and

$$\exp(\Theta \Delta t) = \exp(-\zeta \omega \Delta t) \begin{bmatrix} \cos \omega_d \Delta t & \sin \omega_d \Delta t \\ -\sin \omega_d \Delta t & \cos \omega_d \Delta t \end{bmatrix}$$

3.2 Control Algorithms

To minimize the performance index J(t) given by Eq. (2), subjected to the constraint in Eq. (12), the Hamiltonian H is obtained as

$$H = \underset{\sim}{z}^T(t)\, Q\, \underset{\sim}{z}(t) + \underset{\sim}{u}^T(t)\, R\, \underset{\sim}{u}(t)$$

$$+ \underset{\sim}{\lambda}^T \left[\underset{\sim}{z}(t) - T\, \underset{\sim}{d}\,(t-\Delta t) - \frac{\Delta t}{2} B\, \underset{\sim}{u}(t) - \frac{\Delta t}{2} W_1\, \underset{\sim}{\ddot{x}}_o(t) \right] \tag{20}$$

where:

$\underset{\sim}{\lambda}$ = Lagrange multiplier vector

Q and R = Weighting matrices

The necessary conditions for minimizing the performance index J(t) are:

$$\frac{\partial H}{\partial \underset{\sim}{z}} = 0\,; \quad \frac{\partial H}{\partial \underset{\sim}{u}} = 0\,; \quad \frac{\partial H}{\partial \underset{\sim}{\lambda}} = 0$$

These three matrix equations can be written as

$$2Q\, \underset{\sim}{z}(t) + \underset{\sim}{\lambda}(t) = 0 \tag{21}$$

$$2R\, \underset{\sim}{u}(t) - \frac{\Delta t}{2} B^T\, \underset{\sim}{\lambda}(t) = 0 \tag{22}$$

$$\underset{\sim}{z}(t) = T\, \underset{\sim}{d}(t-\Delta t) + \frac{\Delta t}{2} [B\, \underset{\sim}{u}(t) + W_1\, \underset{\sim}{\ddot{x}}_o(t)] \tag{23}$$

3.2.1 Instantaneous Optimal Open-Loop Control

For this case, the control force vector $\underset{\sim}{u}(t)$ is regulated by the excitation alone, i.e.,

$$\underset{\sim}{\lambda}(t) = \underset{\sim}{q}(t) \tag{24}$$

Upon substituting Eq. (24) into Eqs. (21) - (23), the unknown control vector $\underset{\sim}{u}(t)$ can be solved with the result

$$\underset{\sim}{u}(t) = L\, \underset{\sim}{g}(t) \tag{25}$$

$$\text{in which } L = \left[\left(\frac{\Delta t}{2}\right)^2 B^T Q B + R \right]^{-1}$$

$$\underset{\sim}{g}(t) = -\frac{\Delta t}{2} B^T Q\, T\, \underset{\sim}{d}(t-\Delta t) - \left(\frac{\Delta t}{2}\right)^2 B^T Q\, W_1\, \ddot{\underset{\sim}{x}}_o(t)$$

The response state vector $\underset{\sim}{z}(t)$ under the open-loop control is

$$\underset{\sim}{z}(t) = T\, \underset{\sim}{d}\,(t-\Delta t) + \frac{\Delta t}{2} B\, L\, \underset{\sim}{g}(t) + \frac{\Delta t}{2} W_1\, \ddot{\underset{\sim}{x}}_o(t) \tag{26}$$

For a single-degree-of-freedom system as the one used in the experiments, the control force is given by

$$u(t) = \underset{\sim}{c}_1^T\, \underset{\sim}{d}(t-\Delta t) + c_2\, \ddot{x}_o(t) \tag{27}$$

$$\text{Where } \underset{\sim}{c}_1^T = \left[\frac{2m\Delta t\, Q}{4m^2R+\Delta t^2\, Q}\, (\zeta\omega+\omega_d)\,,\ \frac{2m\Delta t\, Q}{4m^2R+\Delta t^2\, Q}\, (\zeta\omega+\omega_d) \right]$$

$$c_2 = \frac{m\Delta t^2\, Q}{4m^2R+\Delta t^2\, Q}$$

In the uncontrolled case, the state vector can be obtained from Eq. (26) by letting u(t) = 0. Thus,

$$\underset{\sim}{z}(t) = T\, \underset{\sim}{d}(t-\Delta t) + \frac{\Delta t}{2} W_1\, \ddot{\underset{\sim}{x}}_o(t) \tag{28}$$

Under instantaneous optimal open-loop control, the state vector is

$$\underset{\sim}{z}(t) = \begin{bmatrix} 1 & 0 \\ 0 & \alpha \end{bmatrix} \left\{ T\, \underset{\sim}{d}(t-\Delta t) + \frac{\Delta t}{2} W_1\, \ddot{\underset{\sim}{x}}_o(t) \right\} \tag{29}$$

in which

$$\alpha = \frac{4m^2R}{4m^2R+\Delta t^2 Q} \tag{30}$$

The coefficient α given in Eq. (30) can be thought of as a reduced velocity factor characterizing control efficiency. From Eq. (30), it can be seen that control efficiency depends only on the parameter Q/R, the ratio of the chosen weighting matrices.

3.2.2 Instantaneous Optimal Closed-Loop Control

Let the control vector $\underset{\sim}{u}(t)$ be regulated by the feedback response state vector $\underset{\sim}{z}(t)$ alone, i.e.,

$$\underset{\sim}{\lambda}(t) = \Lambda \underset{\sim}{z}(t) \tag{31}$$

where:
Λ = Feedback gain matrix

Substituting Eq. (31) into Eqs. (21) - (23), Eq. (21) yields

$$(2Q + \Lambda)\underset{\sim}{z}(t) = 0 \tag{32}$$

from which the unknown gain matrix was obtained for $\underset{\sim}{z}(t) \neq 0$ as

$$\Lambda = -2Q \tag{33}$$

Substituting Eq. (33) into Eq. (22), the control vector $\underset{\sim}{u}(t)$ was obtained as

$$\underset{\sim}{u}(t) = -\frac{\Delta t}{2} R^{-1} B^T Q \underset{\sim}{z}(t) \tag{34}$$

Under instantaneous optimal closed-loop control, the state vector $\underset{\sim}{z}(t)$ was determined from Eq. (23) with the aid of Eq. (34) as

$$\underset{\sim}{z}(t) = [I + (\Delta t/2)^2 B R^{-1} B^T Q]^{-1} \{T \underset{\sim}{d}(t-\Delta t) + \frac{\Delta t}{2} W_1 \ddot{\underset{\sim}{x}}_o(t)\} \tag{35}$$

For a single-degree-of-freedom system, the solution of the control force u(t) is obtained from Eq. (34), that is

$$u(t) = \left[0, -\frac{\Delta t\, Q}{2mR}\right] \begin{bmatrix} x(t) \\ \dot{x}(t) \end{bmatrix} \tag{36}$$

Under instantaneous optimal closed-loop-control, the state vector as determined from Eq. (35) takes the form

$$\underset{\sim}{z}(t) = \begin{bmatrix} 1 & 0 \\ 0 & \alpha \end{bmatrix} \{T\, \underset{\sim}{d}(t-\Delta t) + \frac{\Delta t}{2} W_1\, \ddot{x}_o(t)\} \tag{37}$$

in which

$$\alpha = \frac{4m^2R}{4m^2R+\Delta t^2 Q} \tag{38}$$

3.2.3 Instantaneous Optimal Open-Closed-Loop Control

Let the control vector $\underset{\sim}{u}(t)$ be regulated by both the feedback response state vector $\underset{\sim}{z}(t)$ and the measured excitation vector $\ddot{\underset{\sim}{x}}_o(t)$, i.e.,

$$\underset{\sim}{\lambda}(t) = \bar{\Lambda}\, \underset{\sim}{z}(t) + \bar{\underset{\sim}{q}}(t) \tag{39}$$

The control vector $\underset{\sim}{u}(t)$ can be eliminated by substituting Eq. (22) into Eq. (23), giving

$$\underset{\sim}{z}(t) = T\, \underset{\sim}{d}(t-\Delta t) + \frac{\Delta t}{2}\left[\frac{\Delta t}{4} BR^{-1} B^T \underset{\sim}{\lambda}(t) + W_1\, \ddot{\underset{\sim}{x}}_o(t)\right] \tag{40}$$

Eq. (21) can be rewritten as

$$\underset{\sim}{\lambda}(t) = -Q\,(\underset{\sim}{z}(t) + \underset{\sim}{z}(t)) \tag{41}$$

Replacing the second term of $\underset{\sim}{z}(t)$ by Eq. (40), and substituting Eq. (39) into Eq. (41), one obtains

$$\{Q + \left[\frac{\Delta t^2}{8} QBR^{-1} B^T + I\right]\bar{\Lambda}\}\ \underset{\sim}{z}(t) + Q\left\{T\, \underset{\sim}{d}(t-\Delta t) + \frac{\Delta t}{2} W_1\, \ddot{\underset{\sim}{x}}_o(t)\right\}$$

$$+ \{\frac{\Delta t^2}{8} QBR^{-1} B^T + I\}\, \bar{\underset{\sim}{q}}(t) = 0 \tag{42}$$

in which the I is a (2nx2n) identity matrix. For $\underset{\sim}{z}(t) \neq 0$, the unknowns $\bar{\Lambda}$ and $\bar{\underset{\sim}{q}}(t)$ were obtained from Eq. (42) as

$$\bar{\Lambda} = -\left[\frac{\Delta t^2}{8} QBR^{-1} B^T + I\right]^{-1} Q \tag{43}$$

$$\bar{\underset{\sim}{q}}(t) = \bar{\Lambda}\left[T\,\underset{\sim}{d}(t-\Delta t) + \frac{\Delta t}{2} W_1\,\ddot{\underset{\sim}{x}}_O(t)\right] \tag{44}$$

Thus, the control vector $\underset{\sim}{u}(t)$ and the response state vector $\underset{\sim}{z}(t)$ under instantaneous optimal open-closed-loop control are

$$\underset{\sim}{u}(t) = \frac{\Delta t}{4} R^{-1} B^T\left[\bar{\Lambda}\,\underset{\sim}{z}(t) + \bar{\underset{\sim}{q}}(t)\right] \tag{45}$$

$$\underset{\sim}{z}(t) = \left[I - \frac{\Delta t^2}{8} BR^{-1} B^T \bar{\Lambda}\right]^{-1}\left[I + \frac{\Delta t^2}{8} BR^{-1} B^T \bar{\Lambda}\right]\left\{T\,\underset{\sim}{d}(t-\Delta t) + \frac{\Delta t}{2} W_1\,\ddot{\underset{\sim}{x}}_O(t)\right\} \tag{46}$$

For a single-degree-of-freedom system, by substituting Eq. (44) into Eq. (45), the control force can be expressed by a feedback equation as

$$u(t) = \frac{\Delta t}{4} R^{-1} B^T \bar{\Lambda}\left\{\underset{\sim}{z}(t) + T\,\underset{\sim}{d}(t-\Delta t) + \frac{\Delta t}{2} W_1\,\ddot{x}_O(t)\right\} \tag{47}$$

The $\bar{\Lambda}$ can be computed by Eq. (43). In Eq. (47)

$$\frac{\Delta t}{4} R^{-1} B^T \bar{\Lambda} = \left[0, -\frac{2\,\Delta t\, m}{8Rm^2+\Delta t^2 Q}\right]$$

Under instantaneous optimal open-closed-loop control, the response state vector $\underset{\sim}{z}(t)$ as determined from Eq. (46) has the form

$$\underset{\sim}{z}(t) = \begin{bmatrix} 1 & 0 \\ 0 & \alpha \end{bmatrix}\left\{T\,\underset{\sim}{d}(t-\Delta t) + \frac{\Delta t}{2} W_1\,\ddot{\underset{\sim}{x}}_O(t)\right\} \tag{48}$$

in which

$$\alpha = \frac{4Rm^2}{4Rm^2+\Delta t^2 Q} \tag{49}$$

Comparing Eqs. (49), (38) and (30), it can be seen that the values of α are the same. Although the control algorithms for the instantaneous optimal control are different, the control efficiencies theoretically should be the same with the same Q/R values.

3.2.4 Global Optimal Closed-Loop Control

This control algorithm has been developed in [ref. 1] and it has been verified by experiments. In this study, it will be used as a reference for the purpose of comparing results using various control laws developed above.

To minimize the classical quadratic performance index given in Eq. (1), the actuator displacement $u_c(t)$ is to be found in the form

$$u_c(t) = k_1 x(t) + k_2 \dot{x}(t) \tag{50}$$

in which k_1 and k_2 are feedback gains. For a single-degree-of-freedom system, k_1 and k_2 are [ref. 1]

$$k_1 = \frac{2\cos\alpha}{\beta m} P_{21} \; ; \; k_2 = \frac{2\cos\alpha}{\beta m} P_{22} \tag{51}$$

Where P_{ij} is the ijth component of the 2x2 matrix P satisfying the Riccati matrix equation given by

$$\dot{P} + PA + A^T P - \frac{1}{2} P \underset{\sim}{b} r^{-1} \underset{\sim}{b}^T P + 2Q = 0 \tag{52}$$

where

$$A = \begin{bmatrix} 0 & 1 \\ -\omega^2 & -2\zeta\omega \end{bmatrix}, \quad \underset{\sim}{b} = \begin{bmatrix} 0 \\ -4k_c \cos\alpha / m \end{bmatrix}, \quad r = \beta k_c, \quad Q = \begin{bmatrix} k & 0 \\ 0 & 0 \end{bmatrix}$$

3.3 Time Delay Compensation

In the above derivations, the system under consideration has been idealized. For example, the assumption was made that the control force can be applied at any time instant as desired. In reality, time delay is unavoidable due to on-line computation and to execution of the control force as commanded. Thus, time delay causes unsynchronized application of the control force and this unsynchronization can not only render the control ineffective, but also may cause instability in the system. To insure the success of structure control, time delay compensation should be incorporated into control algorithms. Therefore, it is desirable to modify feedback gains for the state vector so that time delay can be taken into account.

The base acceleration modeling ground motion is more difficult to predict. However, numerical examples show that it is not very sensitive to time delay in control efficiency. Thus, time delay compensation is only considered for the state vector.

It is relatively easy to compensate for time delay when the controlled structural motion can be assumed to oscillate with the dominant frequency ω in a time interval between each force command. If the displacement feedback force lags displacement by t_x in time while velocity

feedback force lags velocity by $t_X^{\cdot}$ in time, and let $\underset{\sim}{s}$ be the modified feedback gain vector with time delay compensation for the real system, it can be shown that $\underset{\sim}{s}$ is related to the ideal feedback gain vector $\underset{\sim}{k}$ by

$$\underset{\sim}{s}^T = \underset{\sim}{k}^T C \tag{53}$$

where:
C = Compensation matrix

For a single-degree-of-freedom system, the matrix C has the form

$$C = \frac{1}{\cos \omega (t_X - t_X^{\cdot})} \begin{bmatrix} \cos \omega t_X^{\cdot} & \frac{1}{\omega} \sin \omega t_X \\ -\omega \sin \omega t_X^{\cdot} & \cos \omega t_X \end{bmatrix} \tag{54}$$

3.4 Instantaneous Optimal Open-Loop Control with Measured State Variables

As shown in Section 3-2, only measurements of the base acceleration are needed for instantaneous optimal open-loop control. However, experimental results indicate that this control algorithm was not successful. Figures 3-1 through 3-3 show the experimental results on the relative displacement in the frequency domain under a sine wave (2 Hz) excitation. It can be seen from Figure 3-1 that the response amplitude decreased at 2 Hz (frequency of excitation), but greatly increased at 3.52 Hz (natural frequency of the structure). From Figure 3-2 and 3-3, which can show the responses obtained by using different 'spans' of the control force, it can be seen that, as the 'span' increases, the response decreases at 2 Hz but greatly increases at 3.52 Hz.

This phenomenon can be largely attributed to the fact that, because of time delay and instruments measurement error in the practical control process, errors were introduced into computation of the vector $\underset{\sim}{d}(t)$ as given by Eq. (12) and these errors were accumulated in the entire control process.

Hence, in order to reduce the effect of these errors in the control computation, vector $\underset{\sim}{d}(t)$ was corrected by using measured state variables. Thus, instead of using Eq. (13), vector $\underset{\sim}{d}(t)$ was determined by Eq. (15). Therefore, the instantaneous optimal open-loop control was modified by using measured state variables in this study.

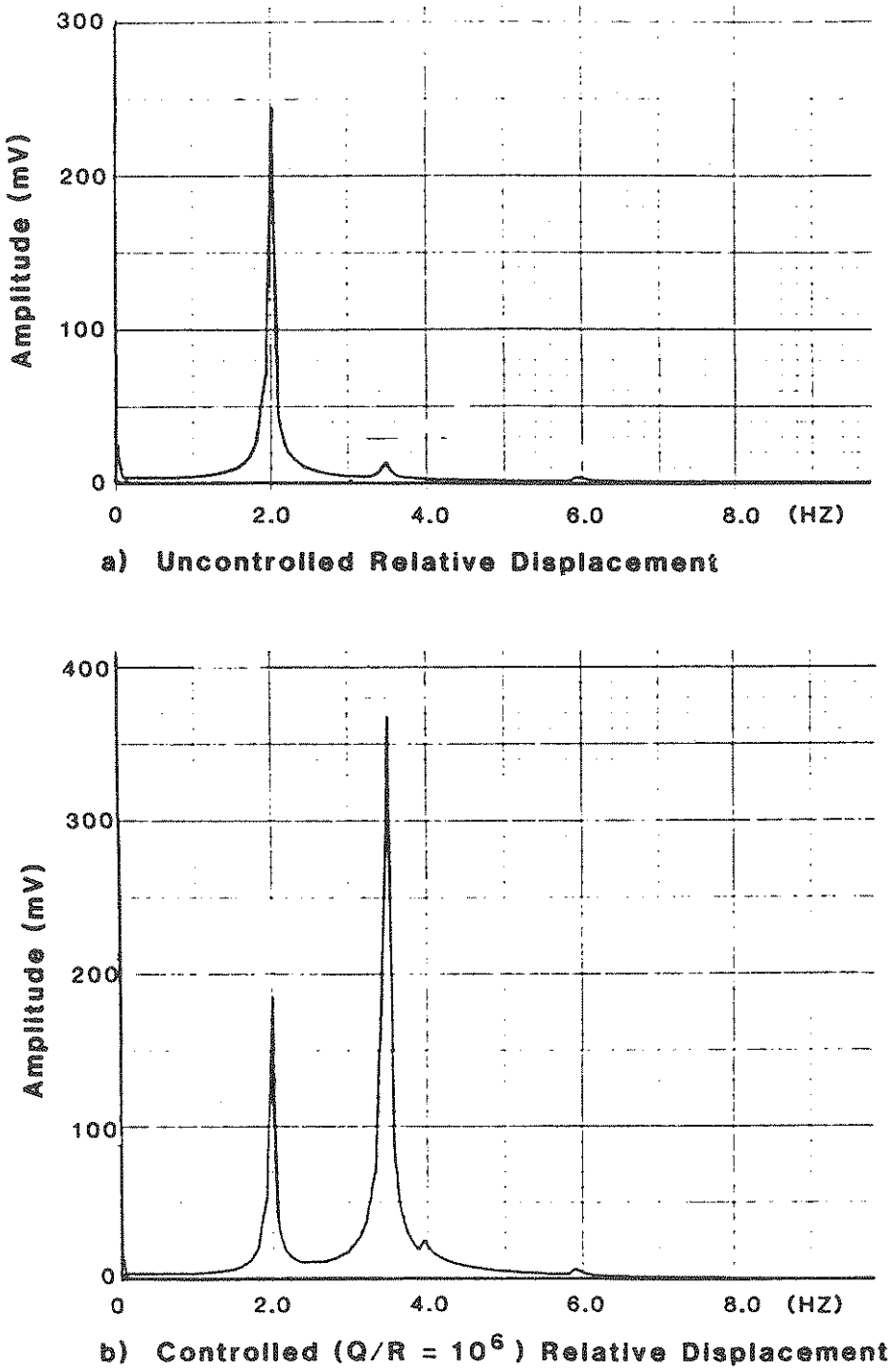

FIGURE 3-1 Instantaneous Open-Loop Control Without Measured State Variables For Sine-Wave (2 HZ) Input

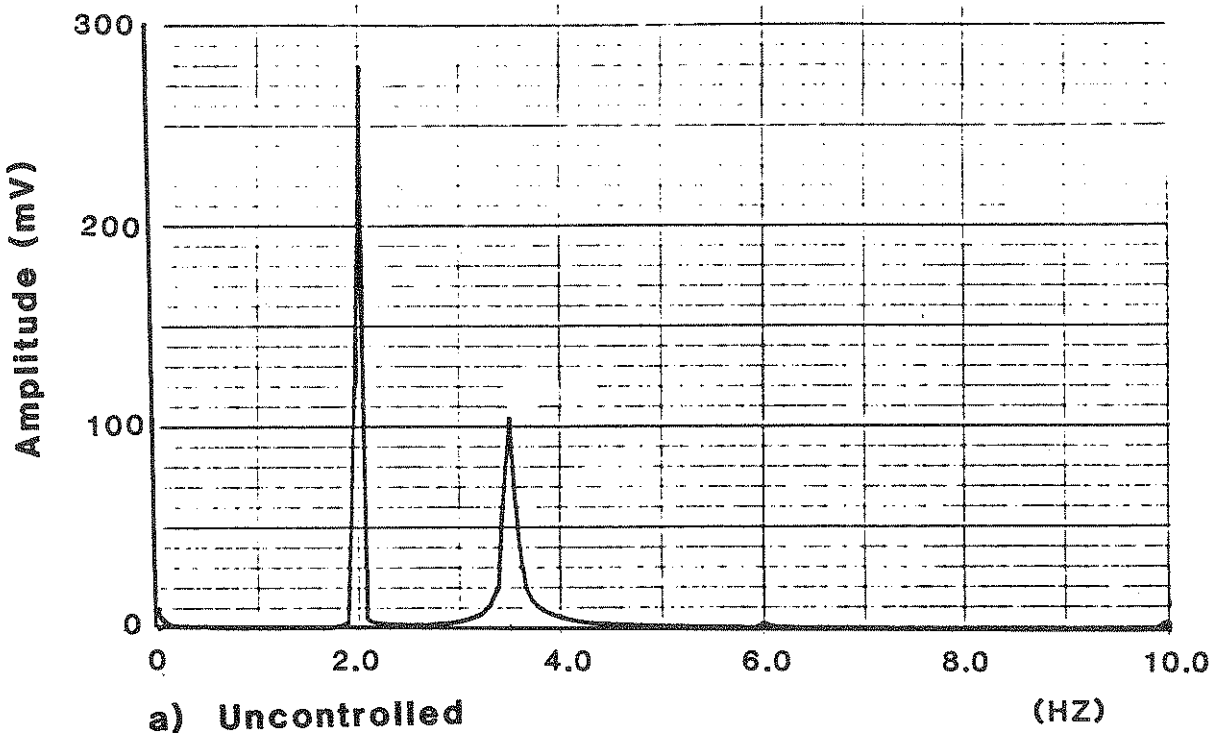

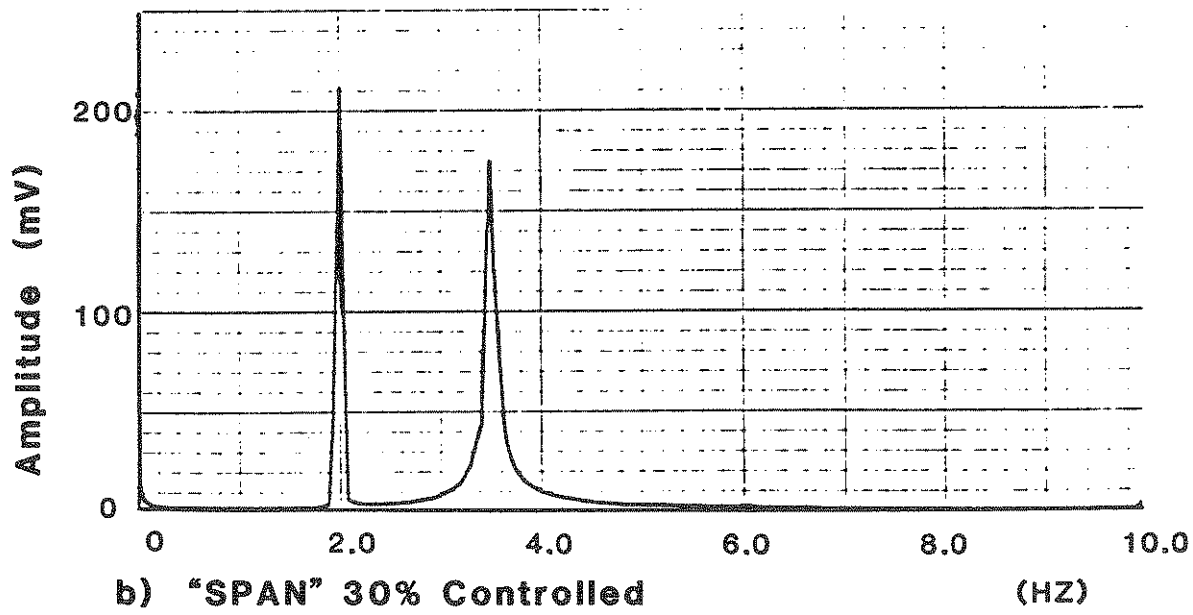

FIGURE 3-2 Open-Loop Control Without Measured State Variables For Different "Span" Controlled Force ($Q/R = 10^7$) For Sine-Wave (2 HZ) Input

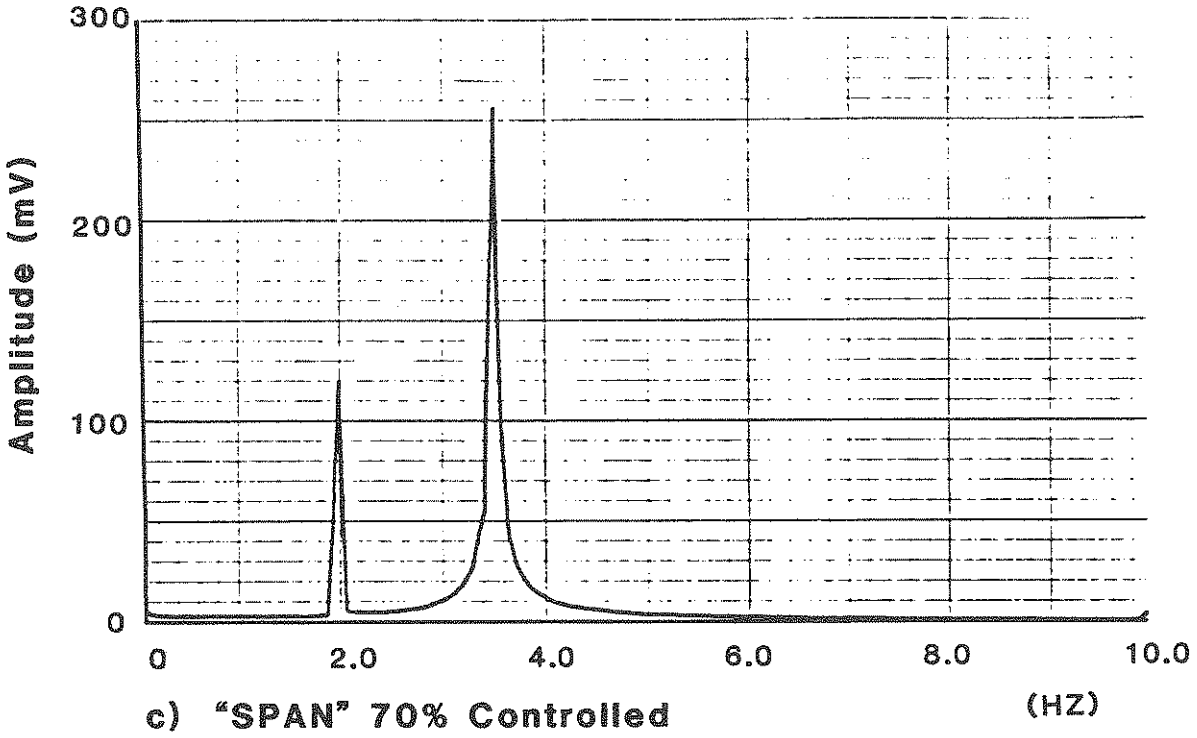

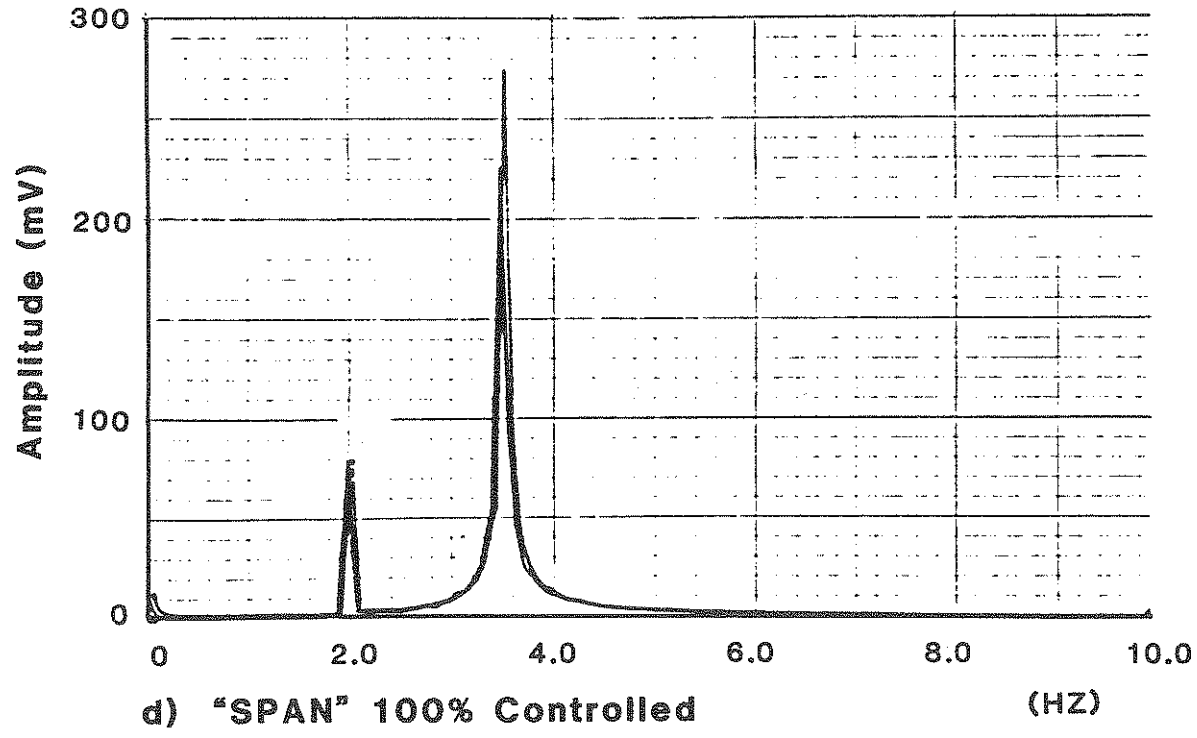

FIGURE 3-3 Open-Loop Control Without Measured State Variables For Different "Span" Controlled Force ($Q/R = 10^7$) For Sine-Wave (2 HZ) Input

SECTION 4
EXPERIMENTAL RESULTS

A comprehensive study of the various control algorithms subjected to three different types of base excitations (sine wave, white noise and earthquake motion) was carried out experimentally and analytically. The designation of the test series is shown in Table 4-I.

TABLE 4-I Designation of Test Series

		Experimental Results		Theoretical Solution	
Input	**Control Algorithm**	**Time Domain**	**Frequency Domain**	**Time Domain**	**Frequency Domain**
Sine wave (2 Hz)	Open	—	SOPFX1	—	SOPFC1
	Open-closed	—	SOCFX1	—	SOCFC1
	Closed	—	—	—	—
	Global	—	—	—	—
White noise (0-10 Hz)	Open	—	WOPFX1	—	WOPFC1
	Open-closed	—	WOCFX1	—	WOCFC1
	Closed	—	WCLFX1	—	WCLFC1
	Global	—	—	—	—
Earthquake 25% EL-CENTRO	Open	$EOPTX_2^1$	$EOPFX_2^1$	$EOPTC_2^1$	$EOPFC_2^1$
	Open-closed	$EOCTX_2^1$	$EOCFX_2^1$	$EOCTC_2^1$	$EOCFC_2^1$
	Closed	$ECLTX_2^1$	$ECLFX_2^1$	$ECLTC_2^1$	$ECLFC_2^1$
	Global	$EGLTX_2^1$	$EGLFX_2^1$	—	—

The notations used in Table 4-I are defined below. Selected experimental results and theoretical solutions including a series of real-time computer simulations are included and discussed in the following sections.

1. Input
   1) Sine Wave (2 Hz) "S"
   2) White Noise (0-10 Hz) "W"
   3) Earthquake Wave (25% EL-CENTRO) "E"
2. Control Algorithms
   1) Uncontrol "UN"
   2) Open-loop Control "OP"
   3) Open-closed-loop Control "OC"
   4) Closed-loop Control "CL"
   5) Global Optimal Control "GL"

3. Domain

1) Time Domain	"T"
2) Frequency Domain	"F"

4. Results

1) Experimental Results	
i) for Relative Displacement	"X1"
ii) for Control Force	"X2"
iii) for Absolute Acceleration	"XA"
2) Theoretical Solution (on-line)	
i) for Relative Displacement	"C1"
ii) for Control Force	"C2"
3) Theoretical Digital Computation	"D"

4-1 Comparison of Experimental Results and Theoretical Solutions

For the three types of input, the uncontrolled responses and open-closed-loop controlled responses are shown in Figures 4-1 through 4-10. Each figure shows the comparison of experimental and theoretical results.

Several remarks can be made:

1. Except for the uncontrolled response under sine wave input, the responses in the theoretical computations are less than the respective experimental responses. Since the theoretical solutions were obtained by using real-time computer simulation, and the time interval for computations and for data acquisition does not fit in all cases the appearance of the peak values, in the base motion the computations always used data equal to or smaller than that actually existing in the structure. Therefore, the theoretical results are always underestimated.
2. For the sine wave input, since the frequency of the sine wave was relatively low, the experimental and theoretical results are close to each other in the uncontrolled case.
3. For the earthquake input, since the relative displacement of the structure and of the prestressing cable was too large in the uncontrolled case, the required compressive stress exceeded the pretensioned stress of the cable, causing loosening of the cable. Therefore, the analytical relative displacement response under the earthquake input in the uncontrolled case is underestimated (Figure 4-3). From Figure 4-4, it can be seen that the natural frequency of the structure was slightly reduced to 3.44 Hz from 3.52 Hz.
4. Figure 4-9(b) shows the real-time simulation results of the control force for the earthquake input. This result was taken from computer output. Since the output signal was not passed through a filter, some high frequency disturbance was introduced into the output signal. This can be seen in Figure 4-10.

4-2. Comparison of Instantaneous Optimal Control and Classical (Global) Optimal Control

As discussed in Section 1, the classical optimal control (global control) can be used only for closed-loop control. For comparison of the control methods, the instantaneous closed-loop control is considered only along with 'global control'.

Choosing the control parameters $\beta = 1$ for classical closed-loop control, and $Q/R = 2.65 \times 10^6$ for instantaneous closed-loop control, the feedback coefficients for determining the control force for both control algorithms are close valued. The experiments were carried out using these control parameters.

Because of the limitations in the experimental resources using these control parameters, both control algorithms could not work for the sine wave input. However, for the white noise input and for the seismic excitation, the control was efficient and the results are shown in Figures 4-11 through 4-13. It can be seen that the instantaneous and the global closed-loop control methods produce very close results using the chosen control parameters.

4-3. Comparison of Different Control Algorithms for Seismic Excitation

For the seismic excitation, the 25% EL-CENTRO acceleration record was used as an input. The time history of the base acceleration is shown in Figure 4-14.

For the instantaneous open-loop control using $Q/R = 2.65 \times 10^6$, the required control force exceeded the limits of experimental resources, so it could not work under these conditions. To prove the feasibility of using this control algorithm under seismic excitation, the control parameter was reduced to $Q/R = 2 \times 10^6$, to carry out the experiments.

The results for each control algorithm under seismic excitation are shown in Table 4-II and in Figures 4-15 through 4-28.

TABLE 4-II Comparison of Control Algorithms for Seismic Excitation

Control Algorithms	Control Parameters	Maximum Control Force lb.	Max. Relative Disp. in.	Reduction %	Max. Absolute Acceleration (first floor) g	Reduction %
Uncontrolled	—	—	0.2	—	0.24	—
Open-loop	$Q/R=2\times10^6$	210	0.075	62.5	—	—
Open-closed Loop	$Q/R=2.65\times10^6$	220	0.075	62.5	0.115	52
Closed-loop	$Q/R=2.65\times10^6$	140	0.075	62.5	0.135	44
Global	$\beta = 1$	160	0.08	60.0	0.128	47

From Table 4-II and figures that are shown in Figures 4-15 through 4-28, it can be seen that the efficiency of instantaneous optimal control compared with classical optimal control is similar 62.5% vs. 60% in displacement reduction and 44% vs. 47% in absolute acceleration reduction. In these experiments, the feasibility of instantaneous optimal control for various excitation including the seismic excitation was verified.

Comparing the different control algorithms for instantaneous optimal control as shown in Figures 4-17 through 4-24, it can be seen that closed-loop control was more efficient than the others. For the closed-loop control, the control force was smaller and the efficiency of control was better. In the open-loop control algorithm and in the open-closed-loop control algorithm, the base acceleration was considered, however, it was not compensated for time delay. Therefore, incorrect values were introduced in the control algorithms, and then the efficiency of control was reduced. In the closed-loop control algorithm, however, the state variables are only considered and since the state variables can be compensated for time delay, it resulted in better efficiency. It was also illustrated that compensation for time delay was necessary.

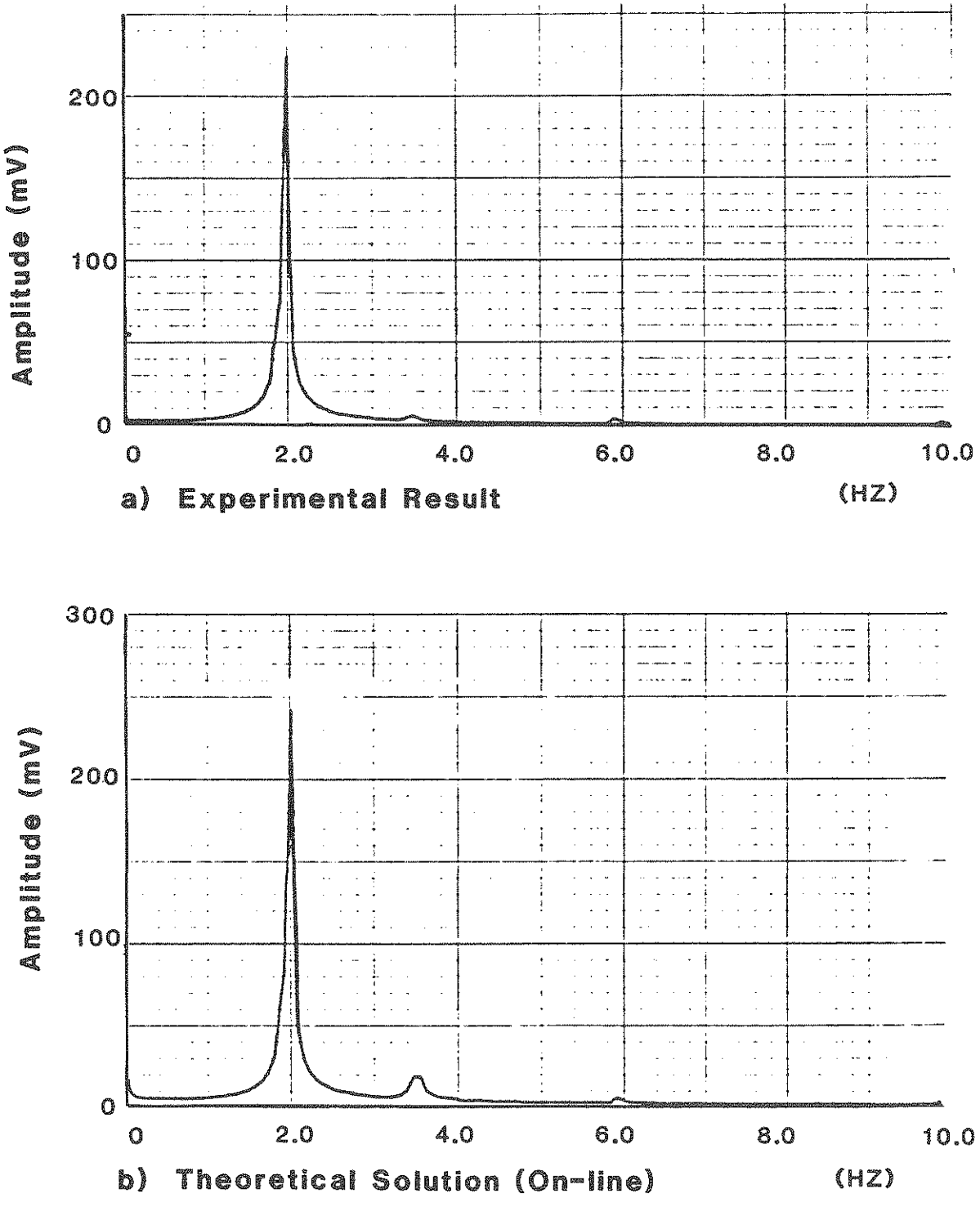

FIGURE 4-1 Uncontrolled Relative Displacement Response In Frequency Domain For Sine-Wave (2 HZ) Input

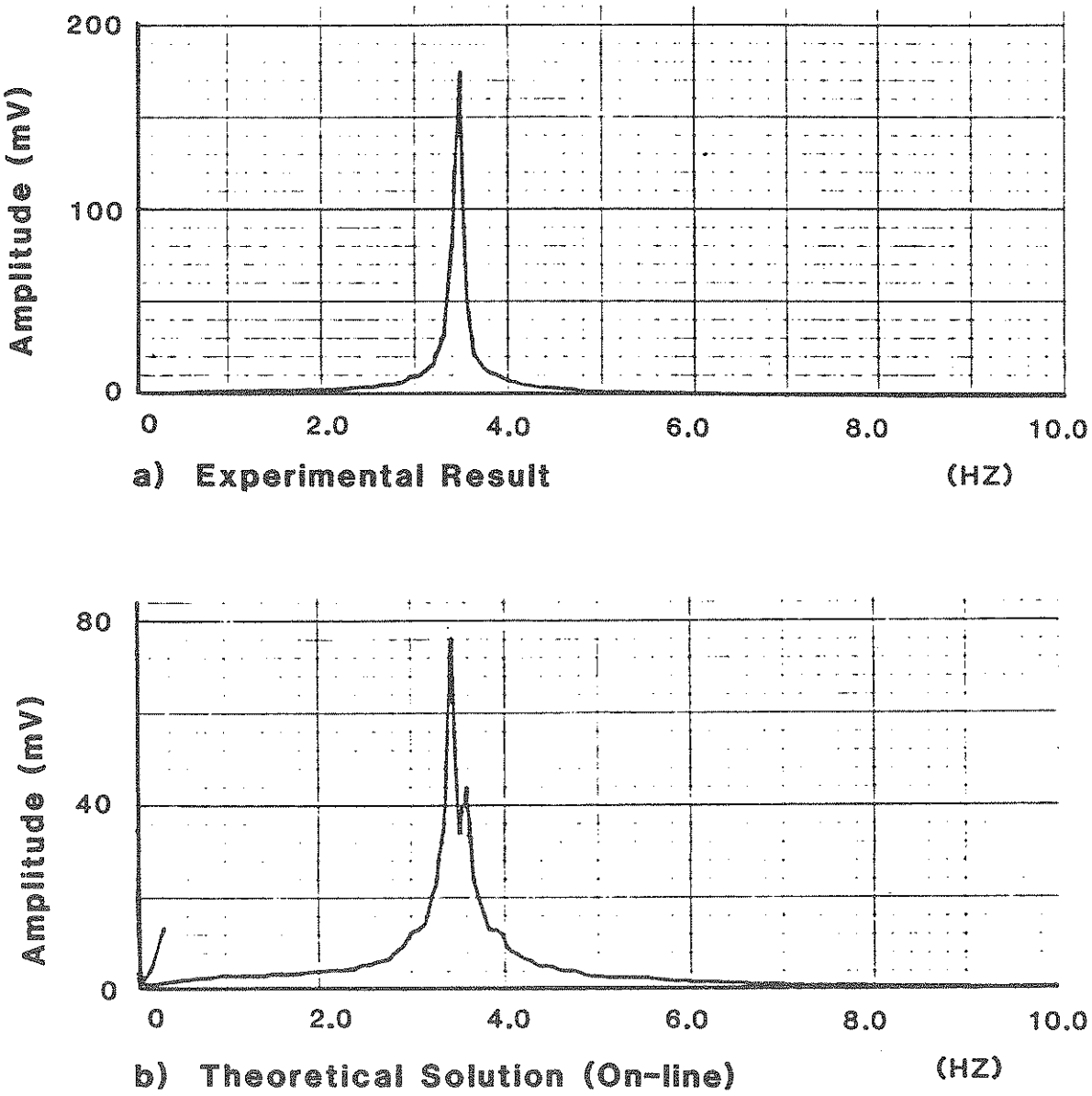

FIGURE 4-2 Uncontrolled Relative Displacement Response In Frequency Domain For White-Noise (0-10 HZ) Input

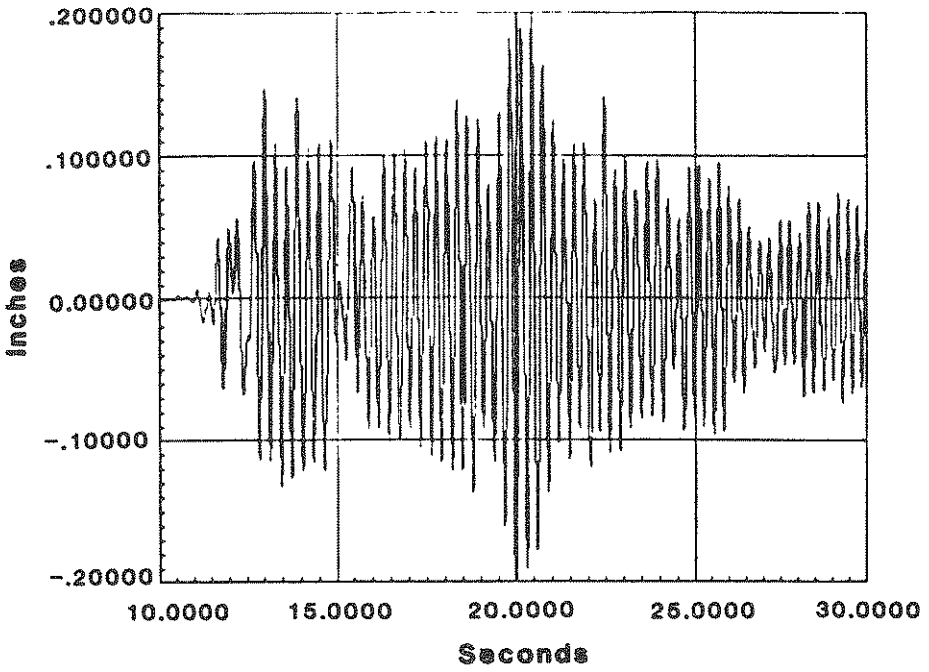

FIGURE 4-3 Uncontrolled Relative Displacement Response In Time Domain For Seismic Input

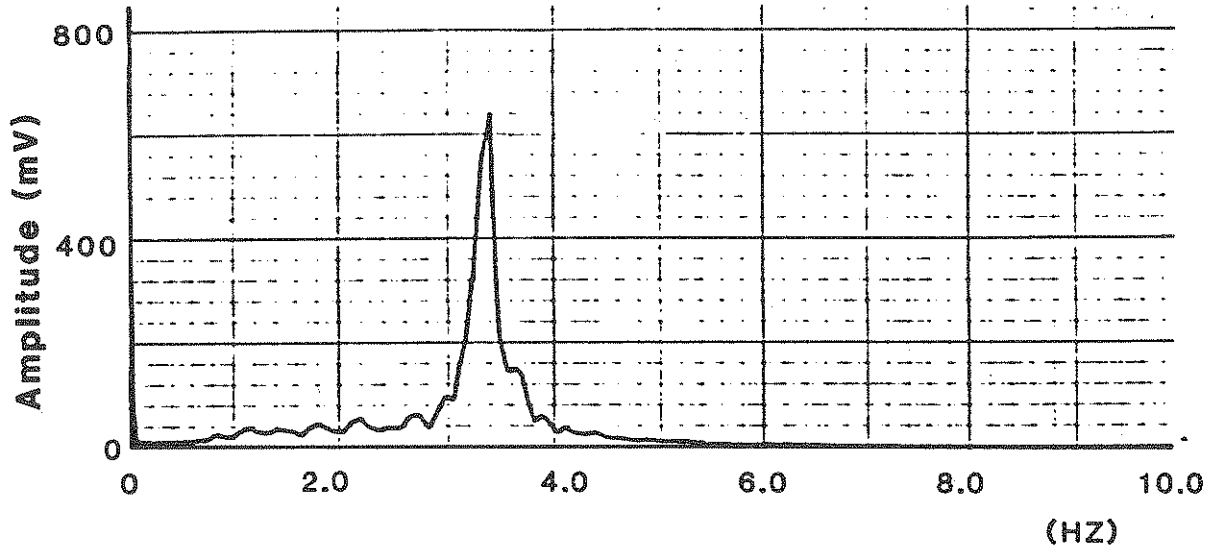

a) Experimental Result

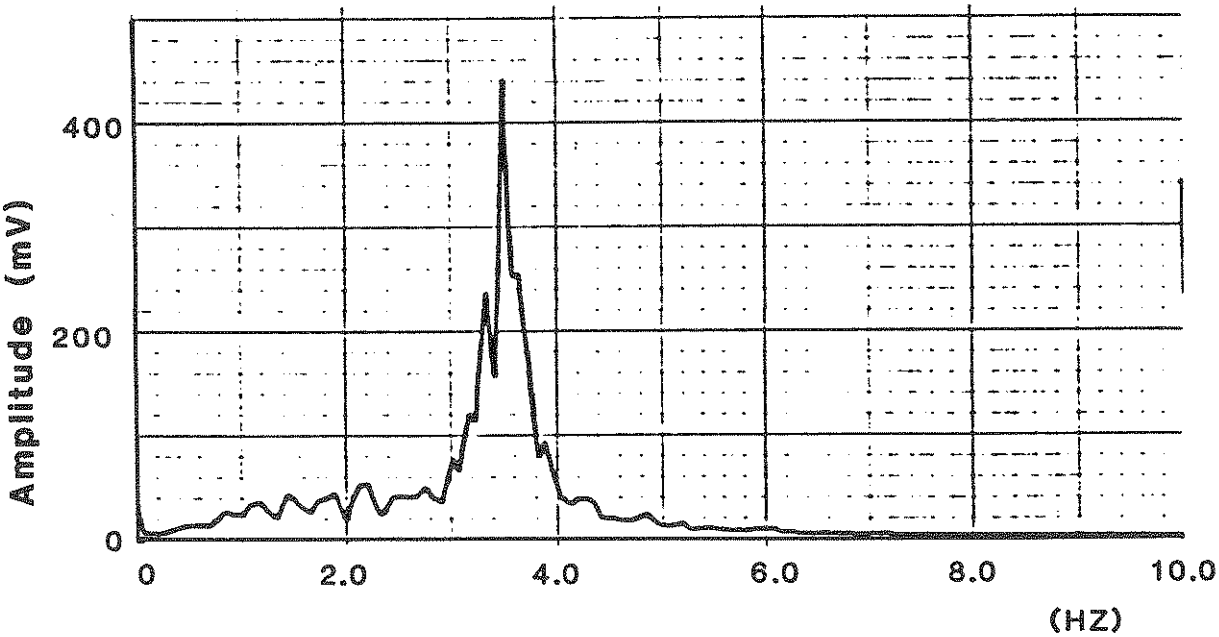

b) Theoretical Solution (On-line)

FIGURE 4-4 Uncontrolled Relative Displacement Response In Frequency Domain For Seismic (25% El-Centro) Input

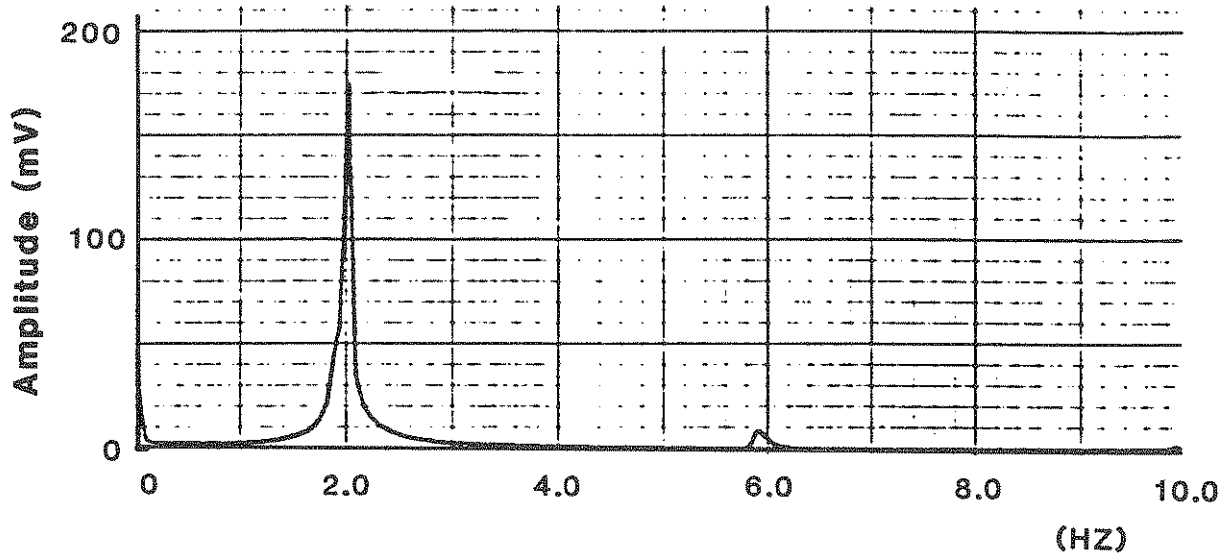

a) Experimental Result

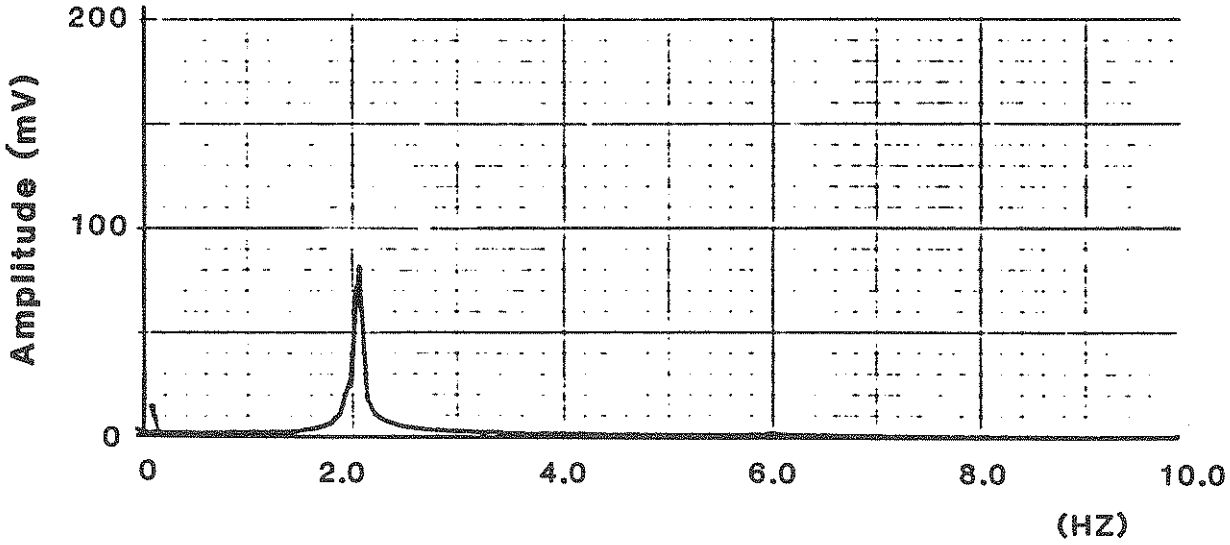

b) Theoretical Solution (On-line)

FIGURE 4-5 Open-Closed-Loop Control ($Q/R = 2.65 \times 10^6$), Relative Displacement Response In Frequency Domain For Sine-Wave (2 HZ) Input

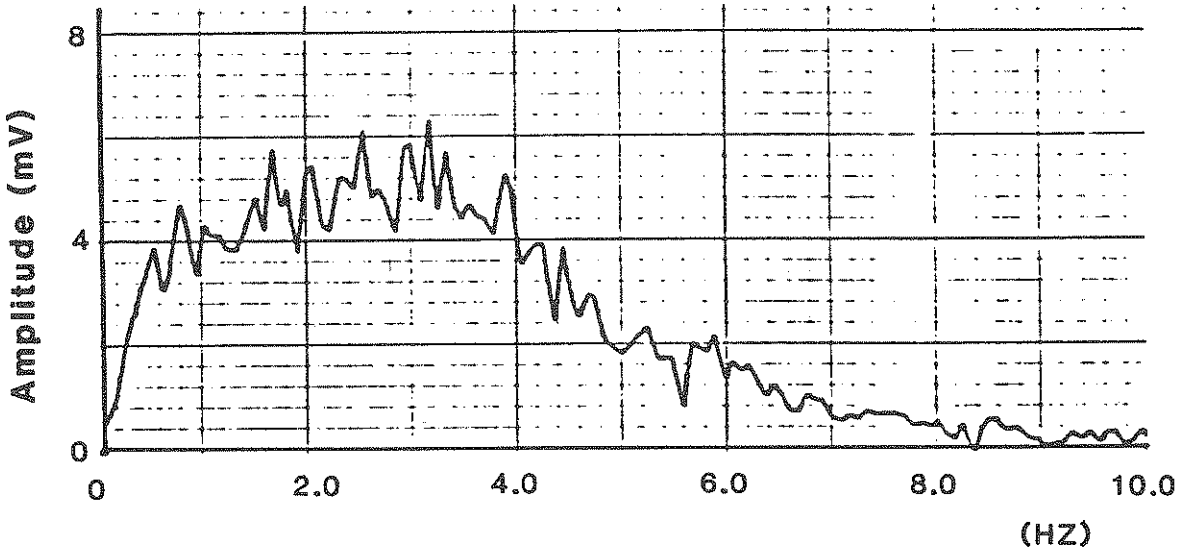

a) Experimental Result

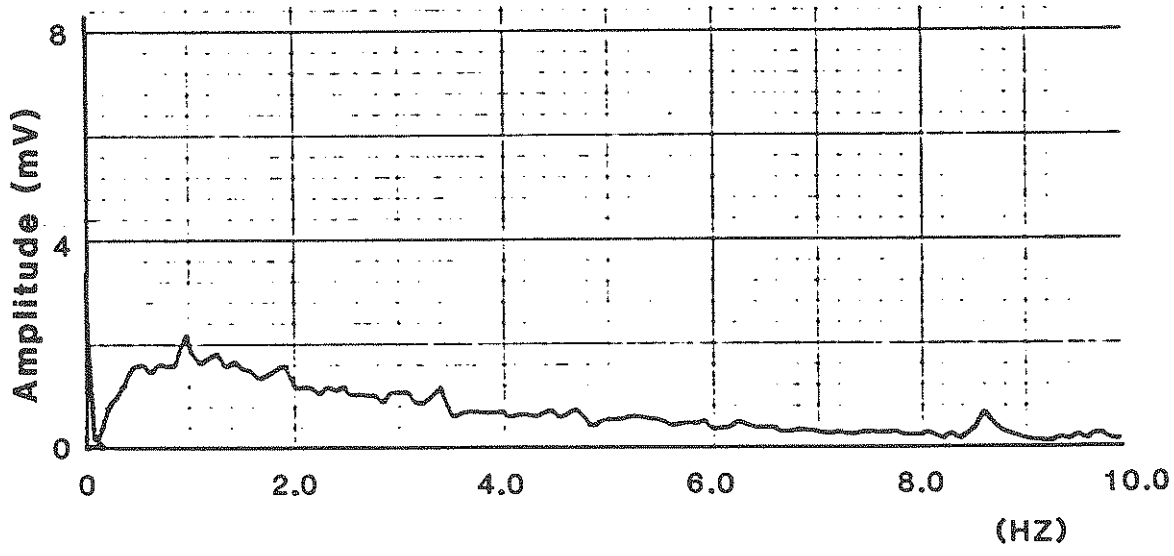

b) Theoretical Solution (On-line)

FIGURE 4-6 Open-Closed-Loop Control ($Q/R = 2.65 \times 10^6$), Relative Displacement Response In Frequency Domain For White Noise (0-10 HZ) Input

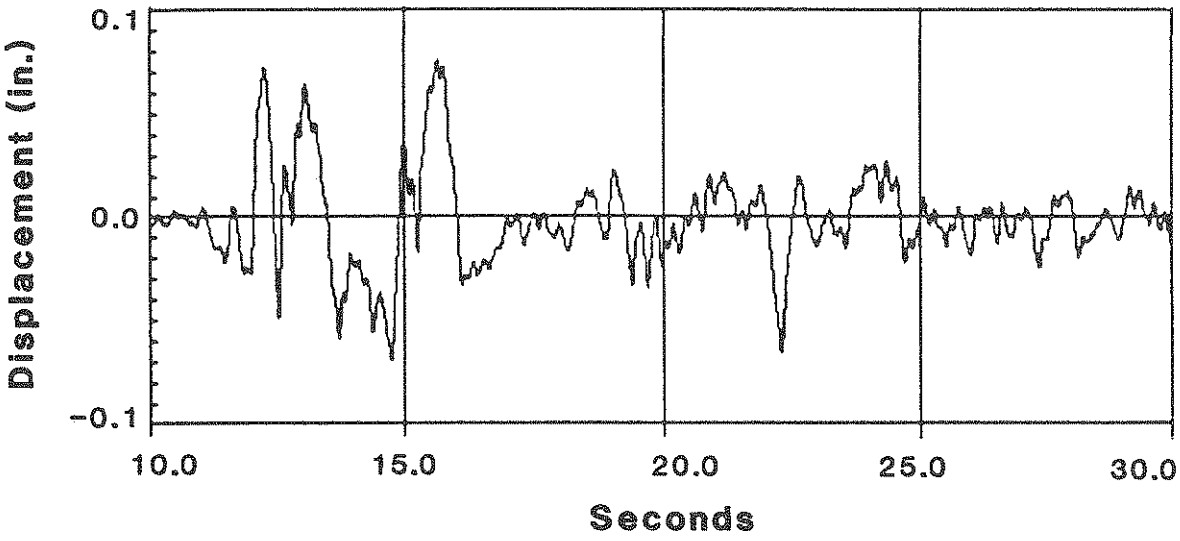

a) Experimental Result

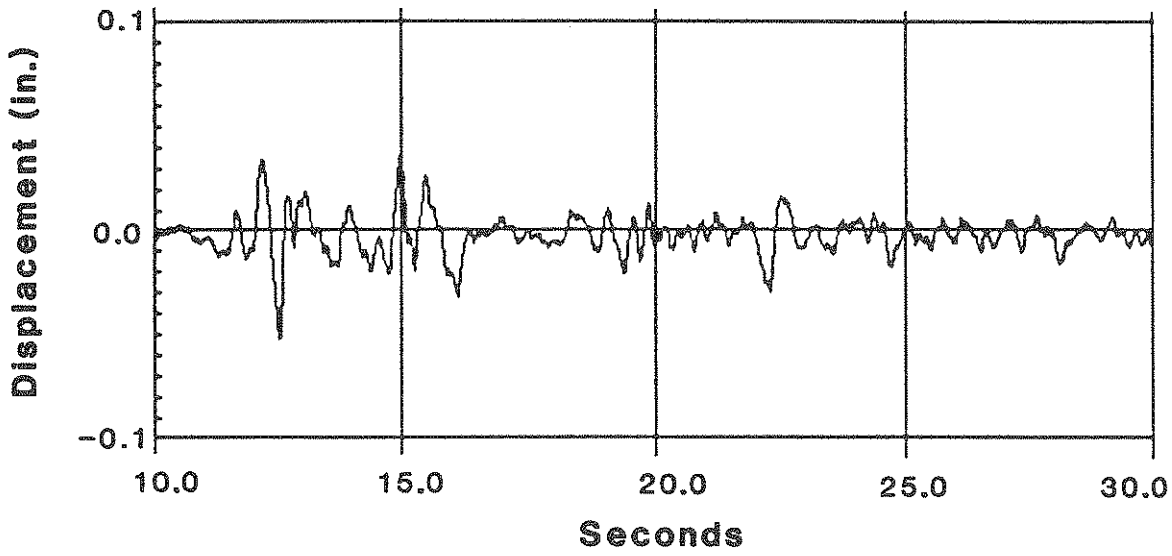

b) Theoretical Solution (On-line)

FIGURE 4-7 Open-Closed-Loop Control ($Q/R = 2.65 \times 10^6$), Relative Displacement Response In Time Domain For Seismic Input

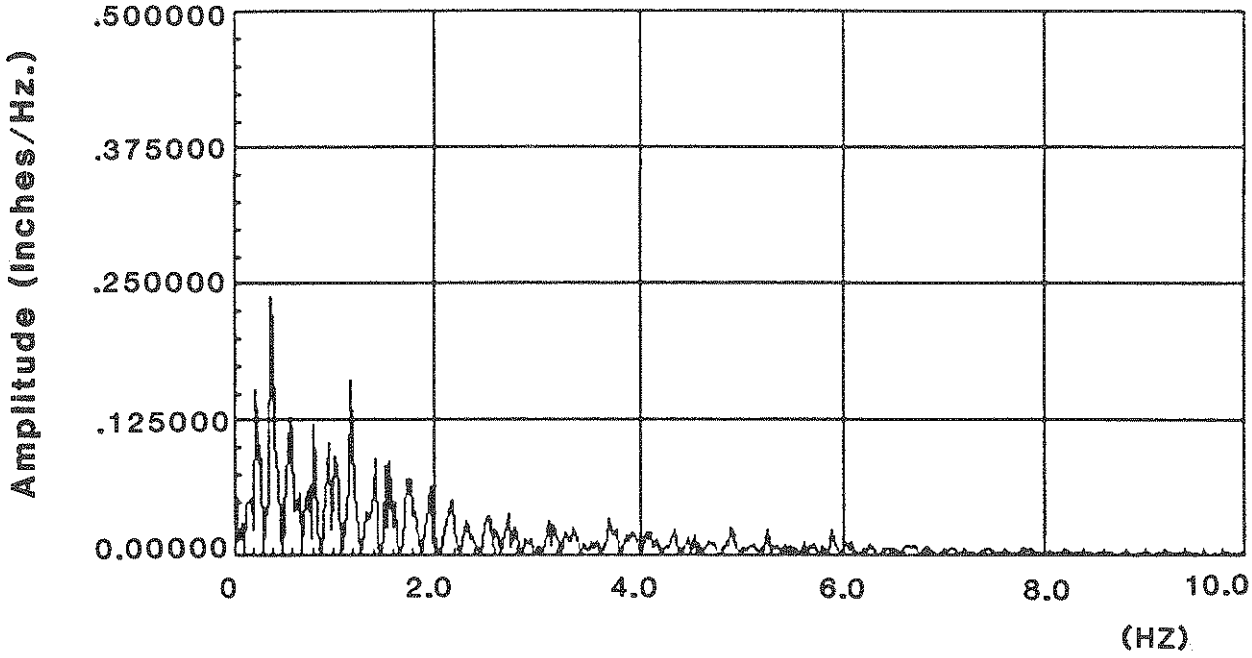

a) Experimental Result

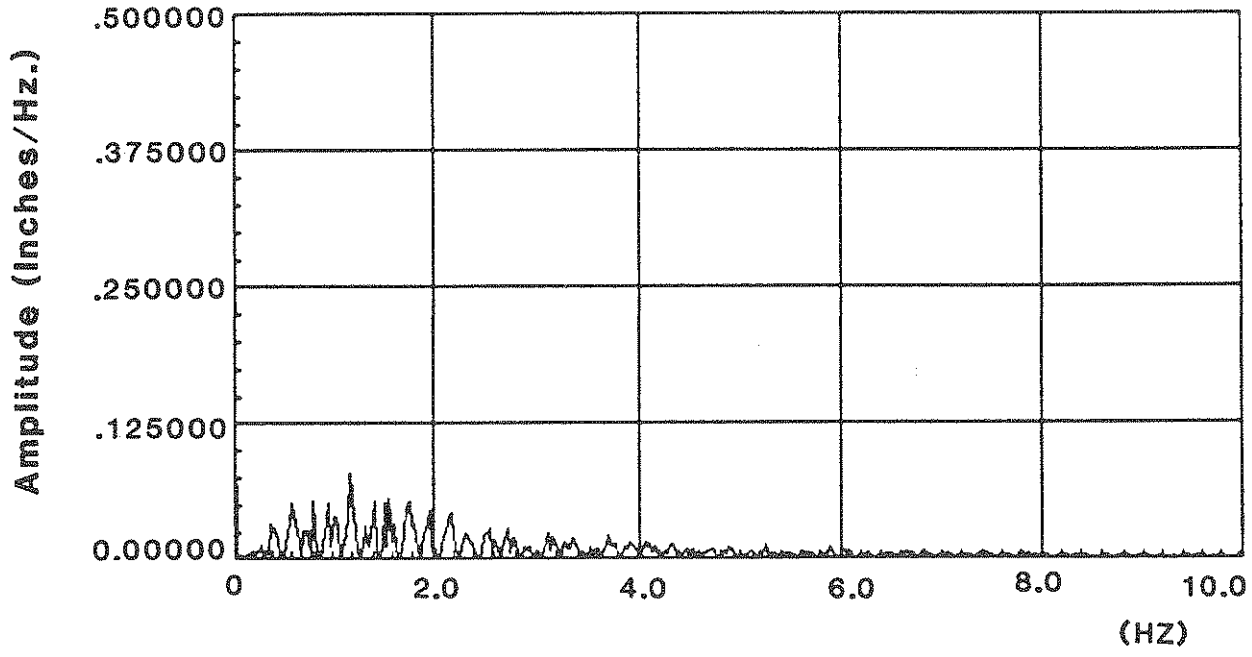

b) Theoretical Solution (On-line)

FIGURE 4-8 Open-Closed-Loop Control ($Q/R = 2.65 \times 10^6$), Relative Displacement Response In Frequency Domain For Seismic Input

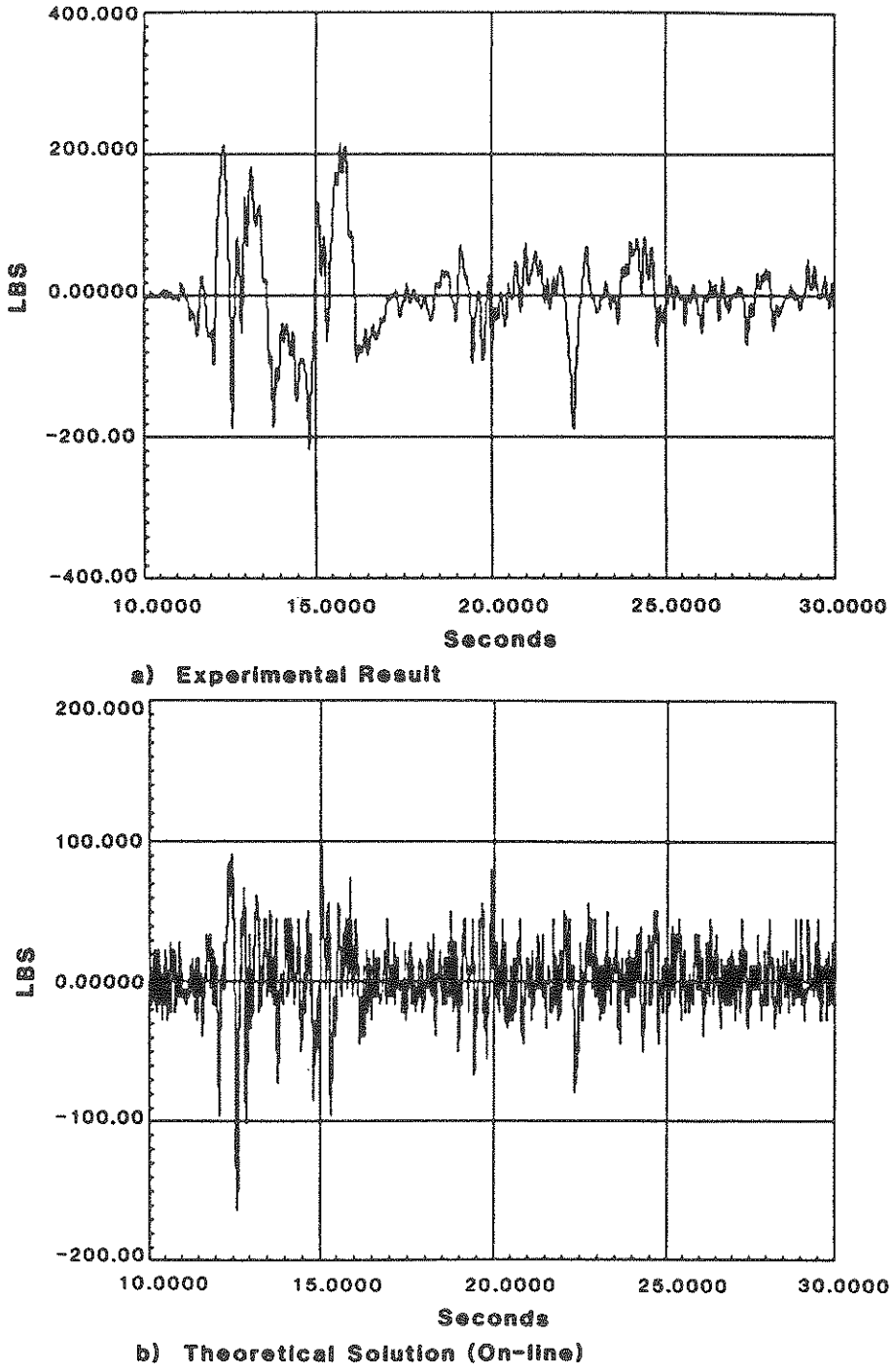

FIGURE 4-9 Open-Closed-Loop Control ($Q/R = 2.65 \times 10^6$), Control Forces In Time Domain For Seismic Input

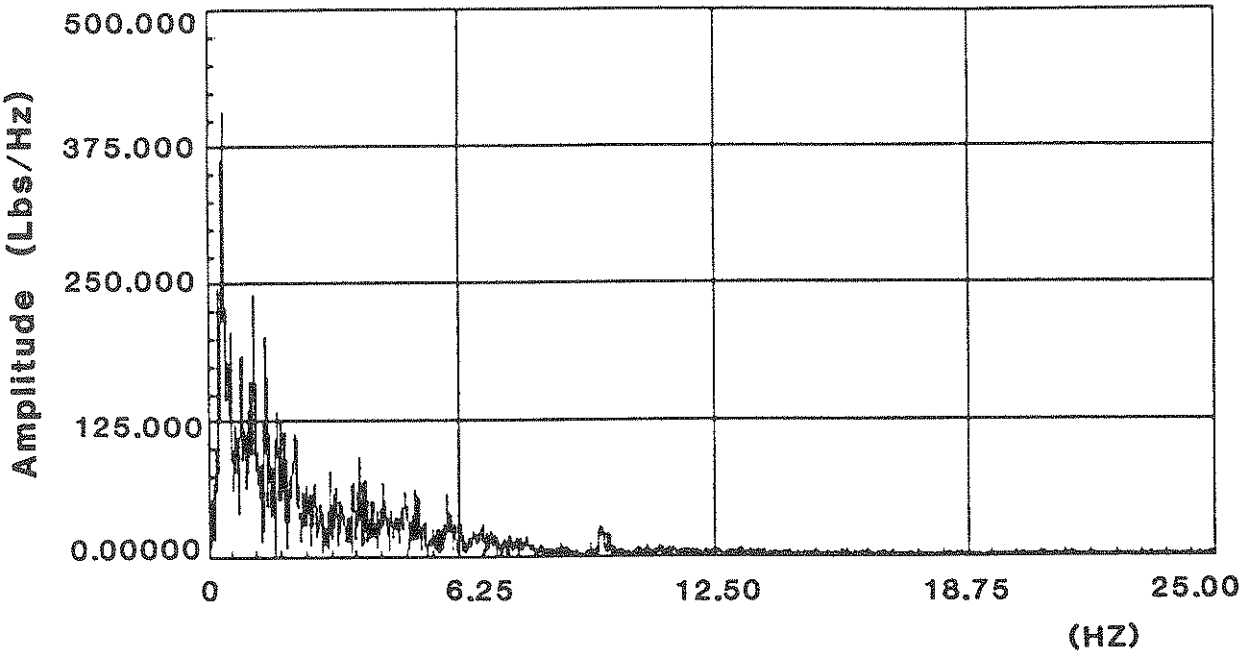

a) Experimental Result

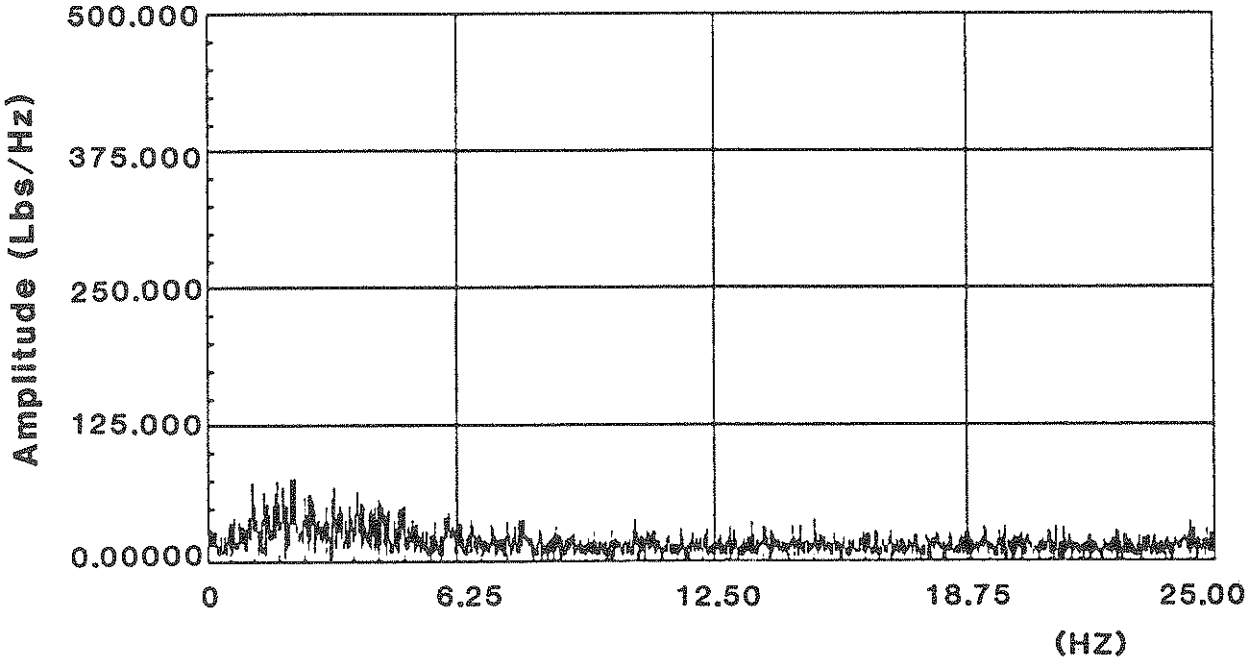

b) Theoretical Solution (On-line)

FIGURE 4-10 Open-Closed-Loop Control ($Q/R = 2.65 \times 10^6$), Control Force In Frequency Domain For Seismic Input

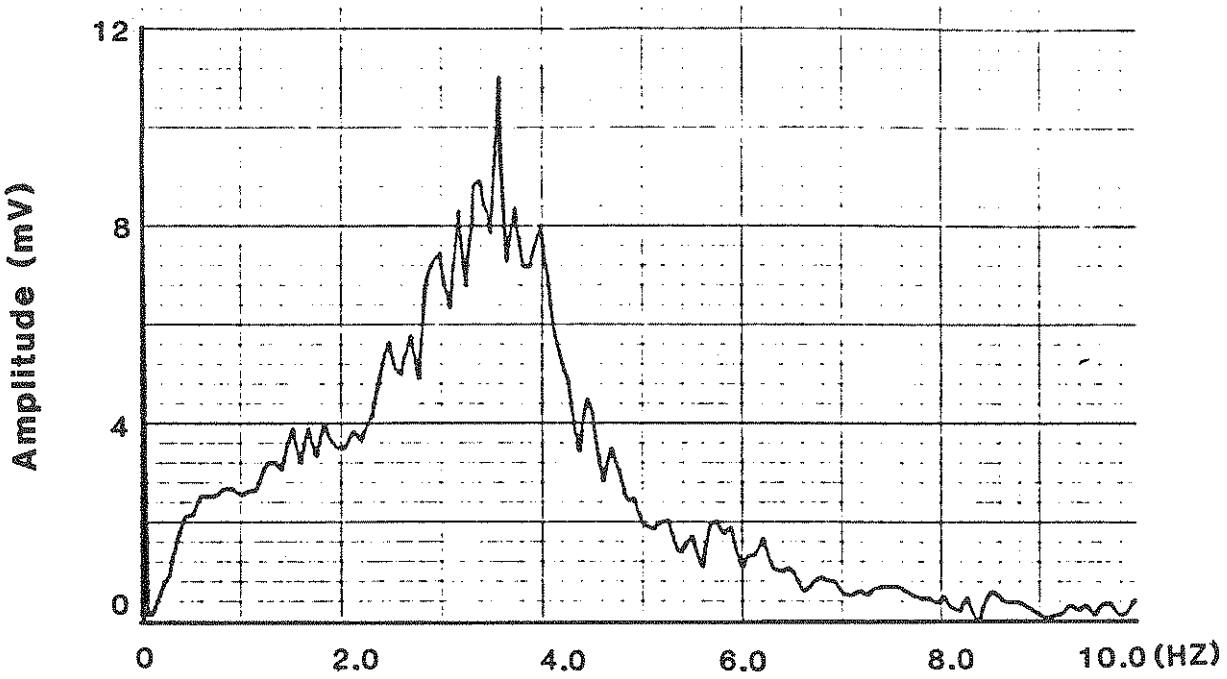

a) Instantaneous Optimal Close-loop Control with ($Q/R = 2.65 \times 10^6$)

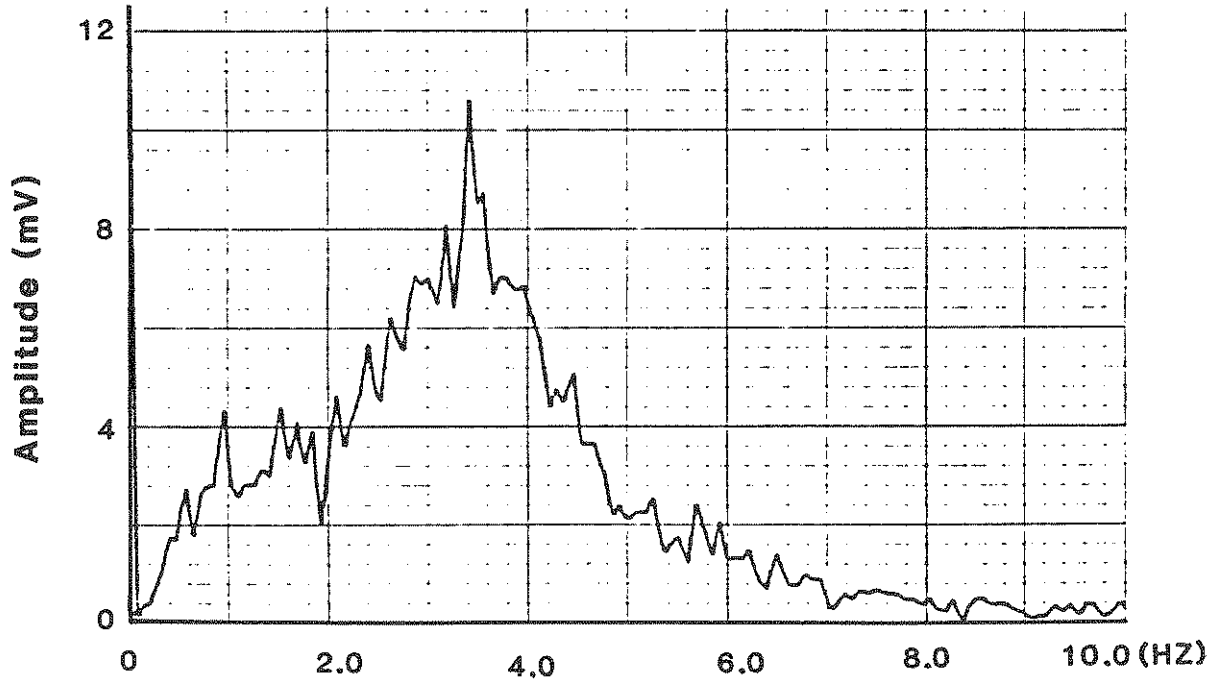

b) Global Closed-loop Control with $\beta = 1$

FIGURE 4-11 Relative Displacement Response In Frequency Domain For White-Noise (0-10 HZ) Input

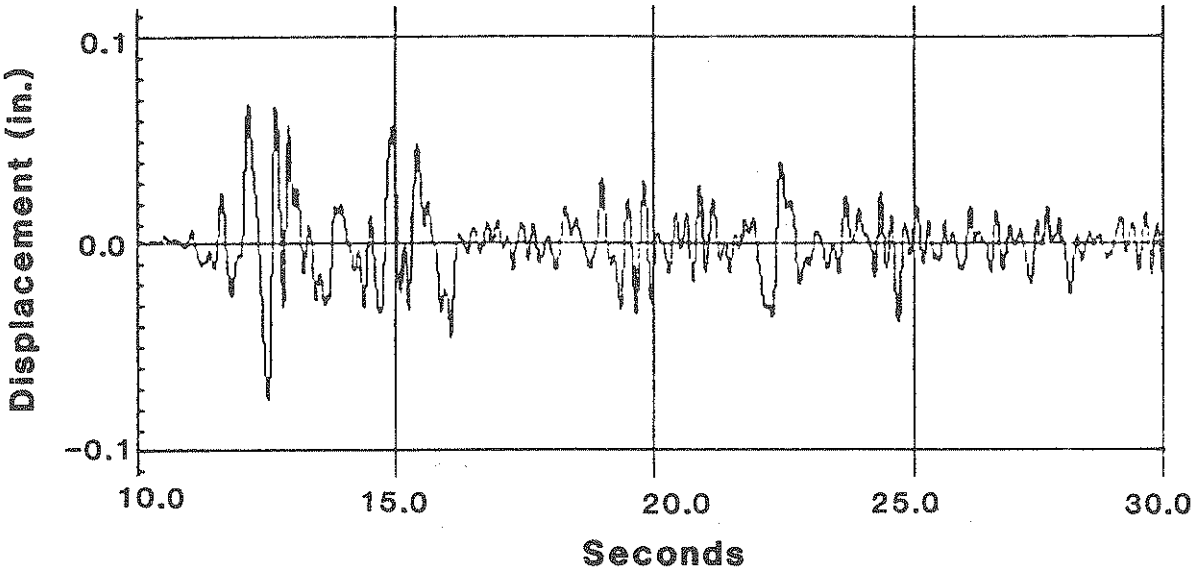

a) Instantaneous Optimal Closed-loop Control with ($Q/R = 2.65 \times 10^6$)

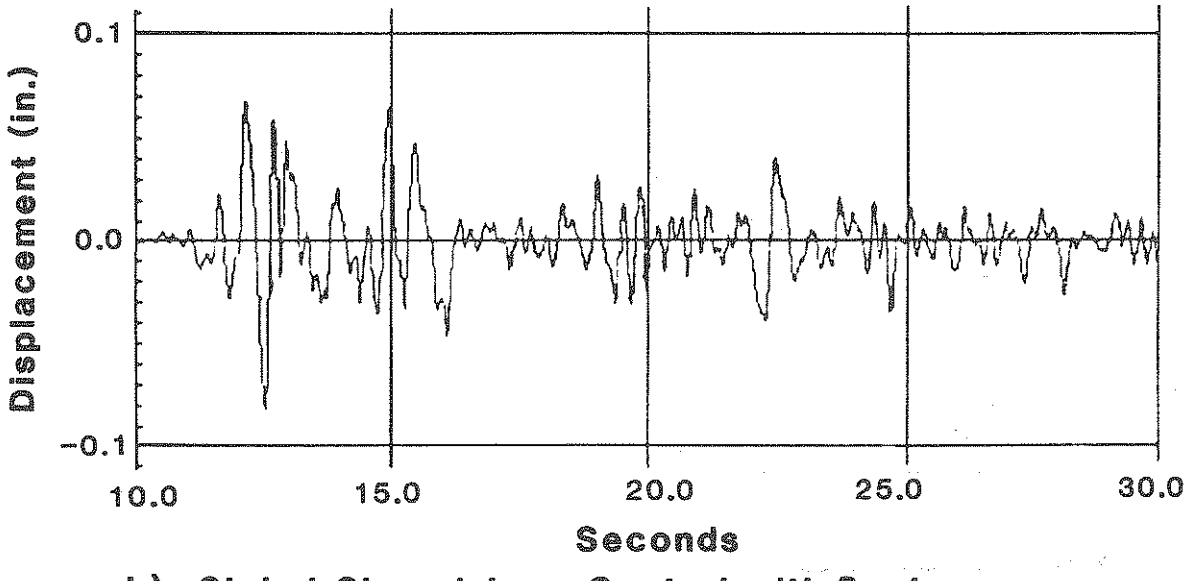

b) Global Closed-loop Control with $\beta = 1$

FIGURE 4-12 Relative Displacement Response In Time Domain For Seismic Input

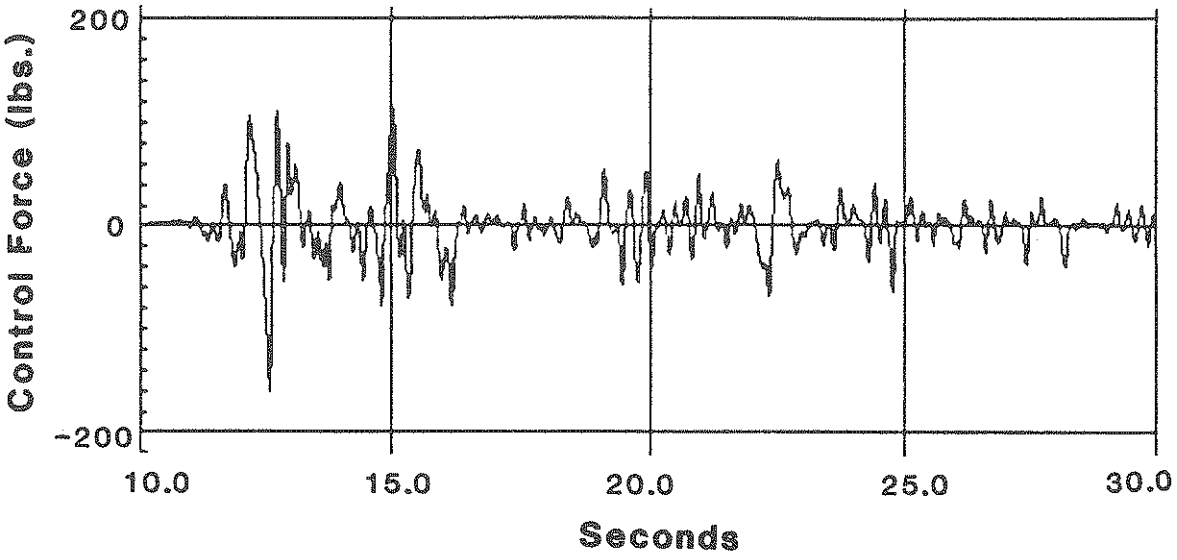

a) Instantaneous Optimal Closed-loop Control with ($Q/R = 2.65 \times 10^6$)

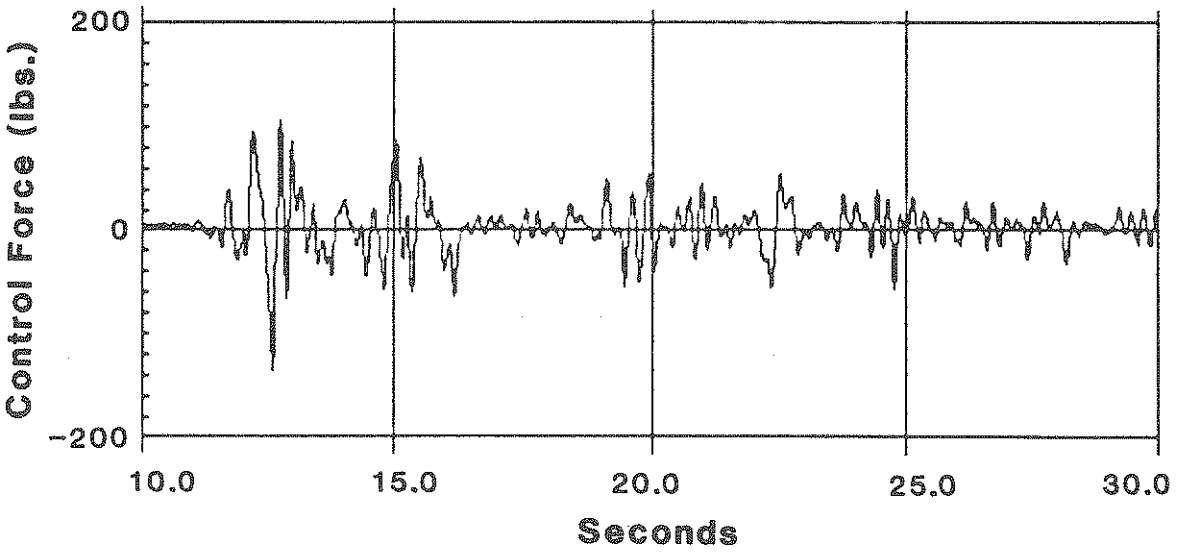

b) Global Closed-loop Control with $\beta = 1$

FIGURE 4-13 Control Forces in Time Domain For Seismic Input

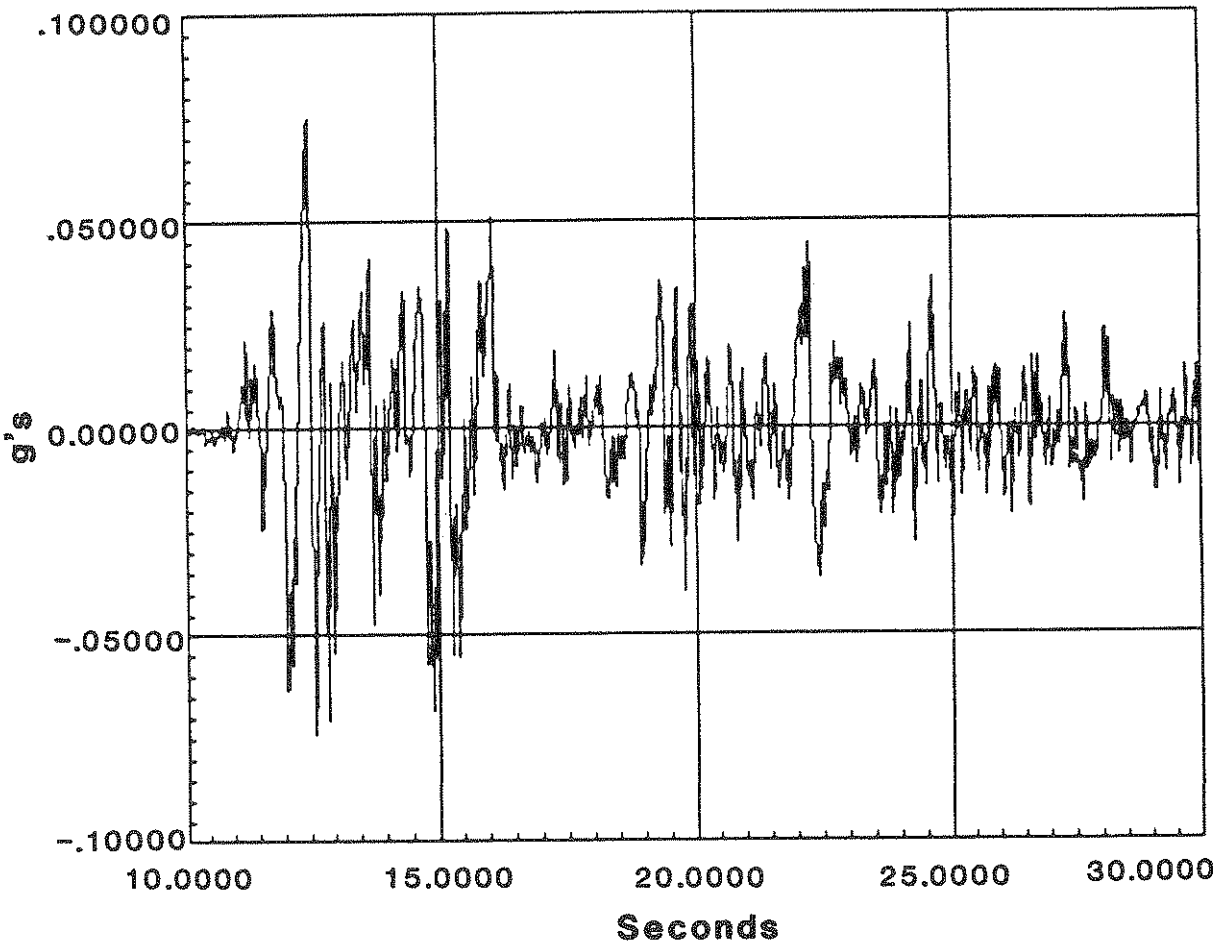

FIGURE 4-14 Time History Of Base Acceleration For Seismic Excitation

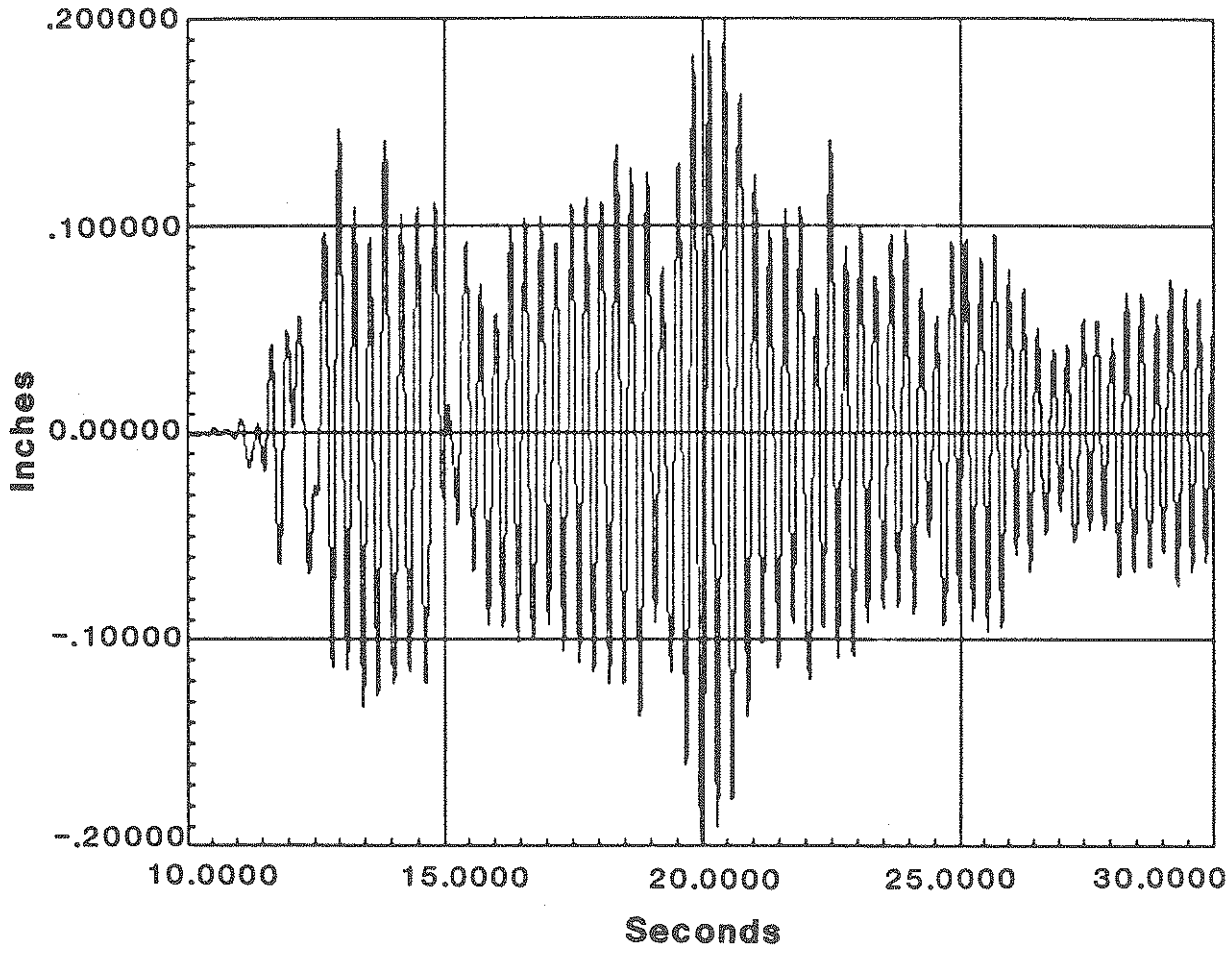

FIGURE 4-15 Experimental Result Of Uncontrolled Relative Displacement Response In Time Domain For Seismic Excitation

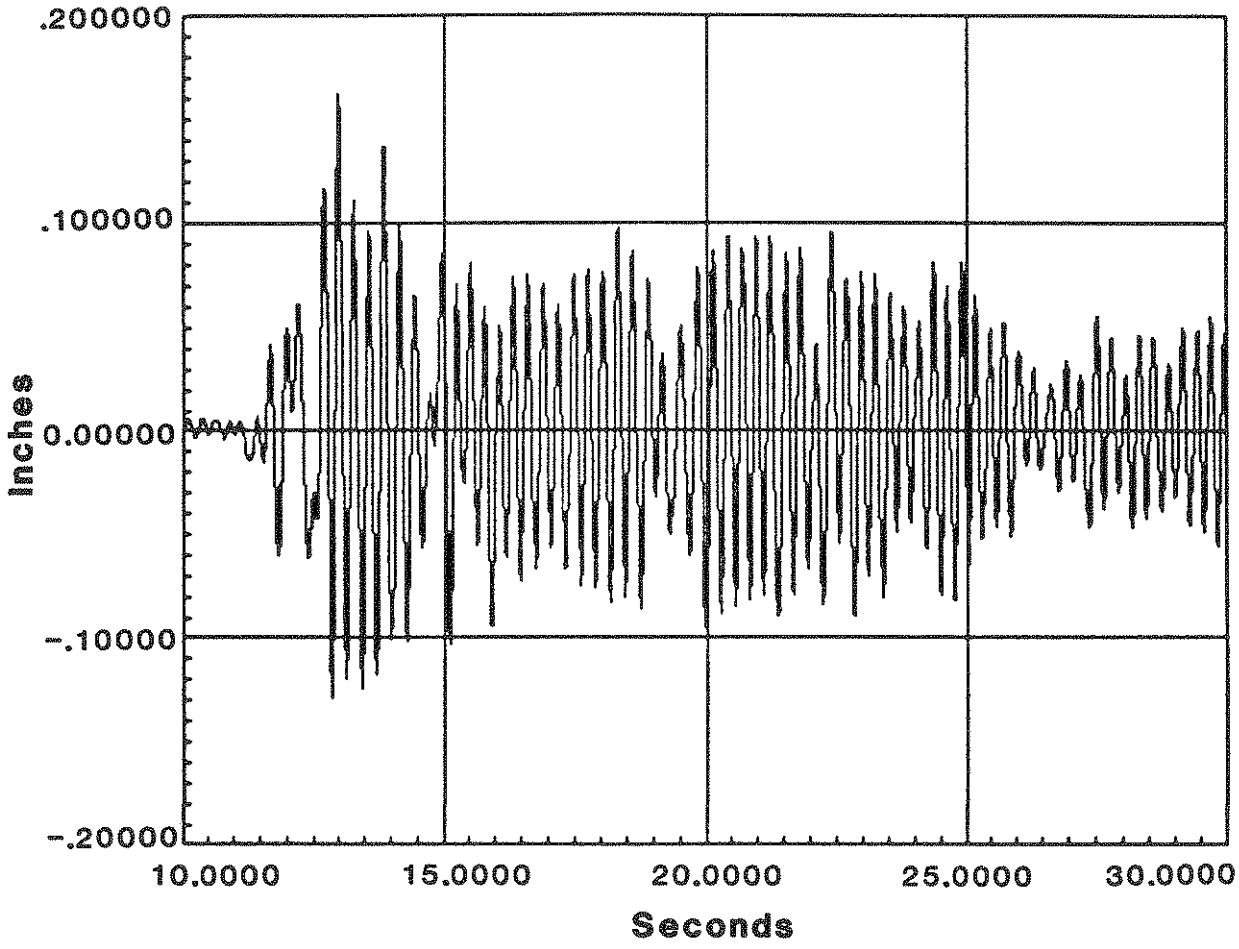

FIGURE 4-16 Theoretical Result Of Uncontrolled Displacement Response In Time Domain For Seismic Excitation

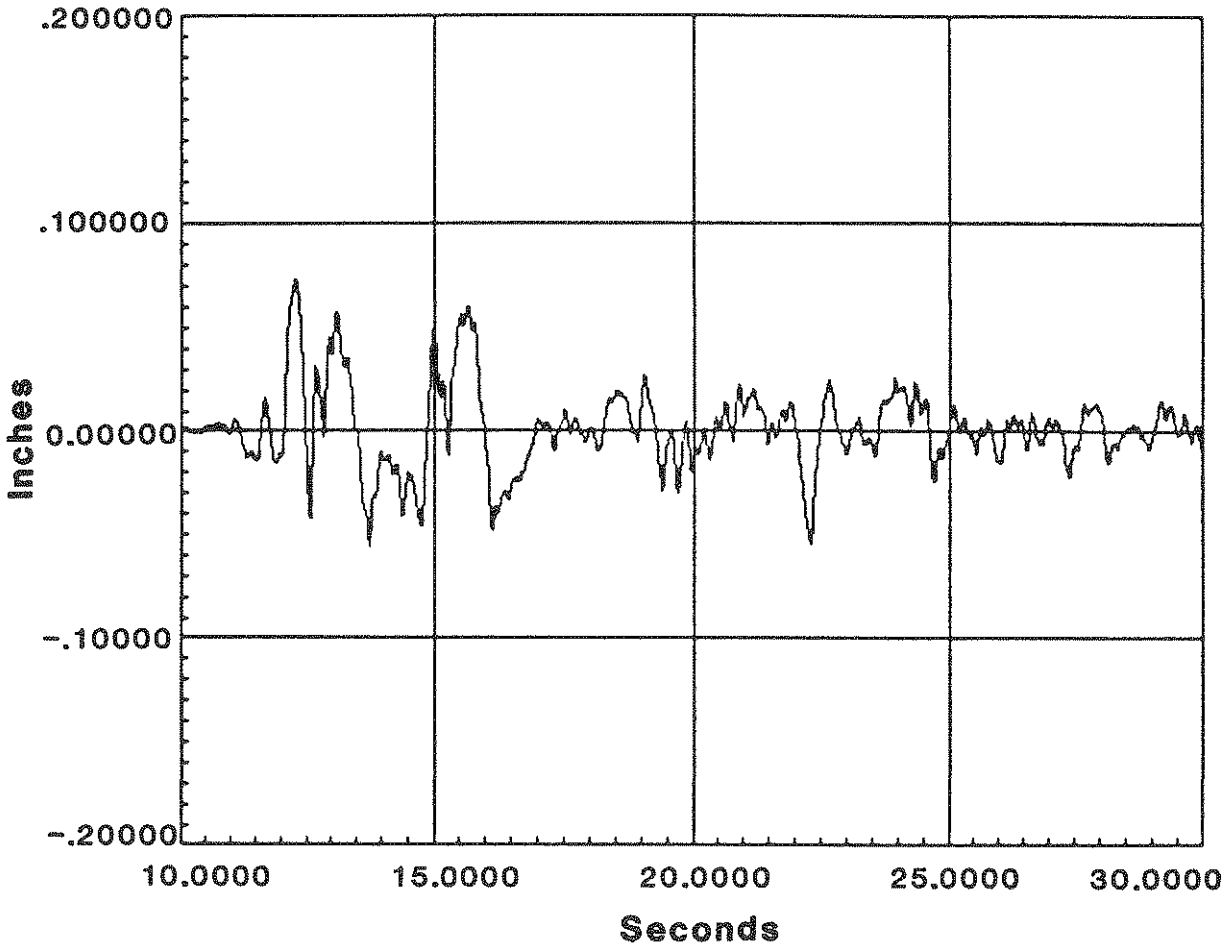

FIGURE 4-17 Relative Displacement Response In Time Domain For Instantaneous Open-Loop Control With $Q/R = 2 \times 10^6$ For Seismic Excitation

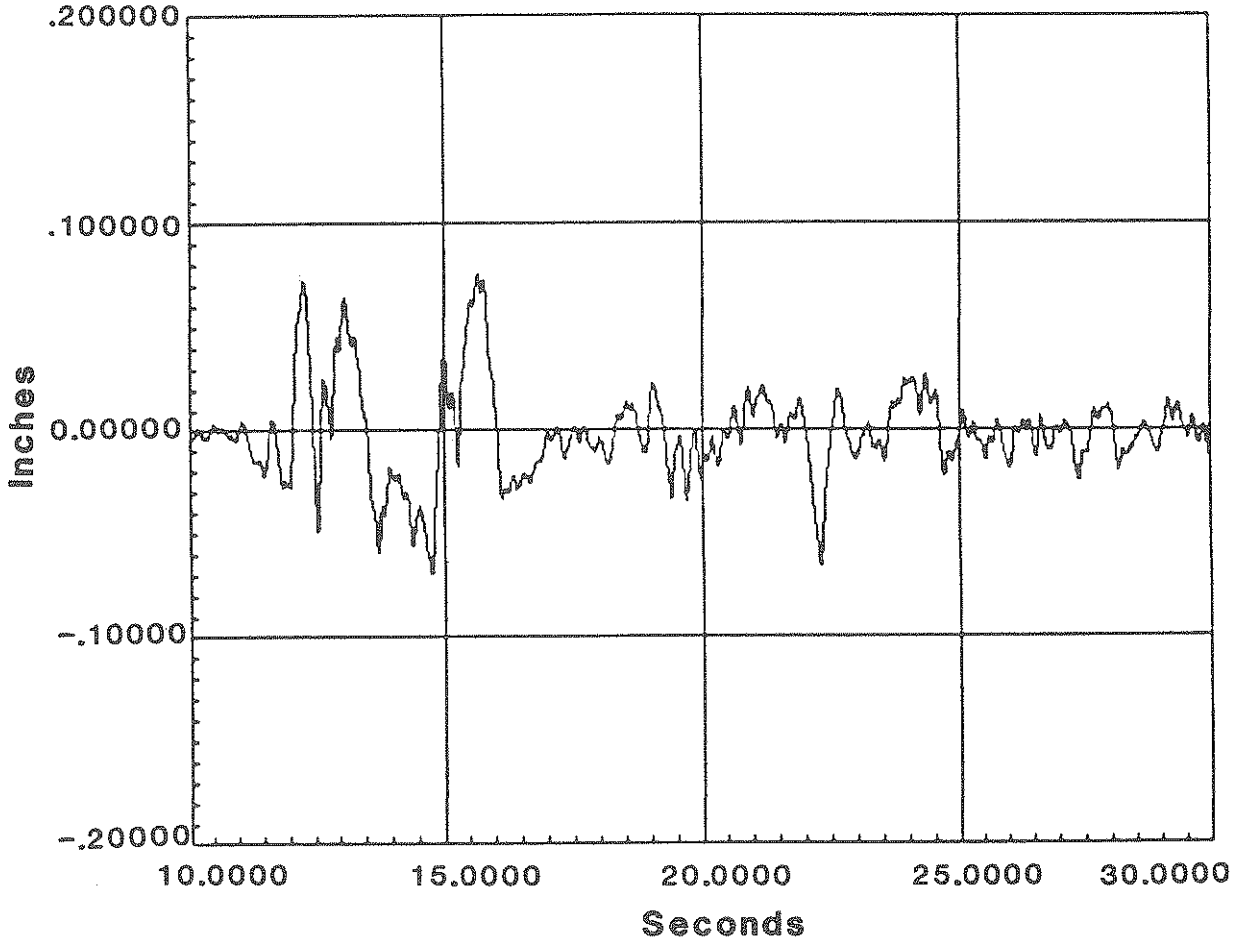

FIGURE 4-18 Relative Displacement Response In Time Domain For Instantaneous Open-Closed Loop Control With $Q/R = 2.65 \times 10^6$ For Seismic Excitation

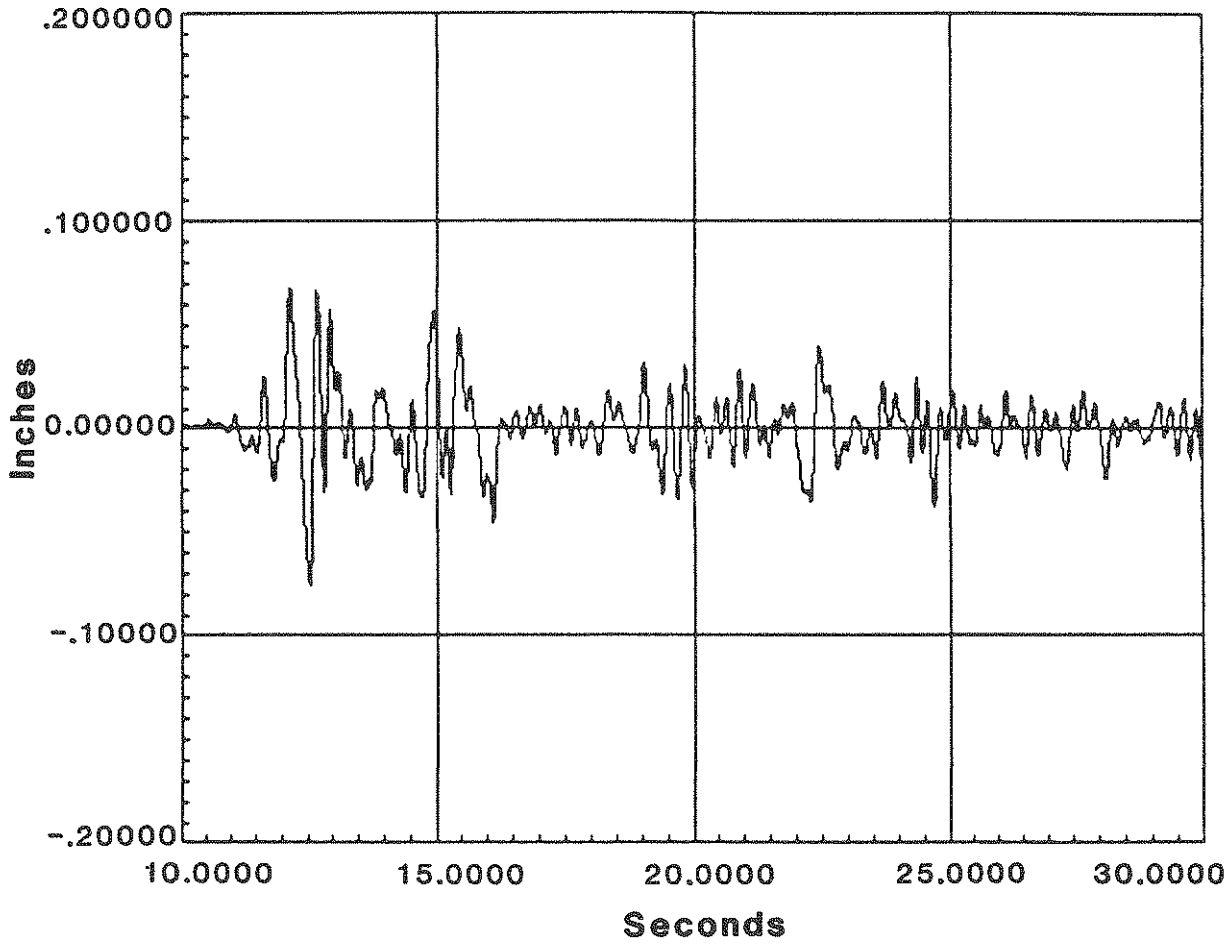

FIGURE 4-19 Relative Displacement Response In Time Domain For Instantaneous Closed-Loop Control With ($Q/R = 2.65 \times 10^6$) For Seismic Excitation

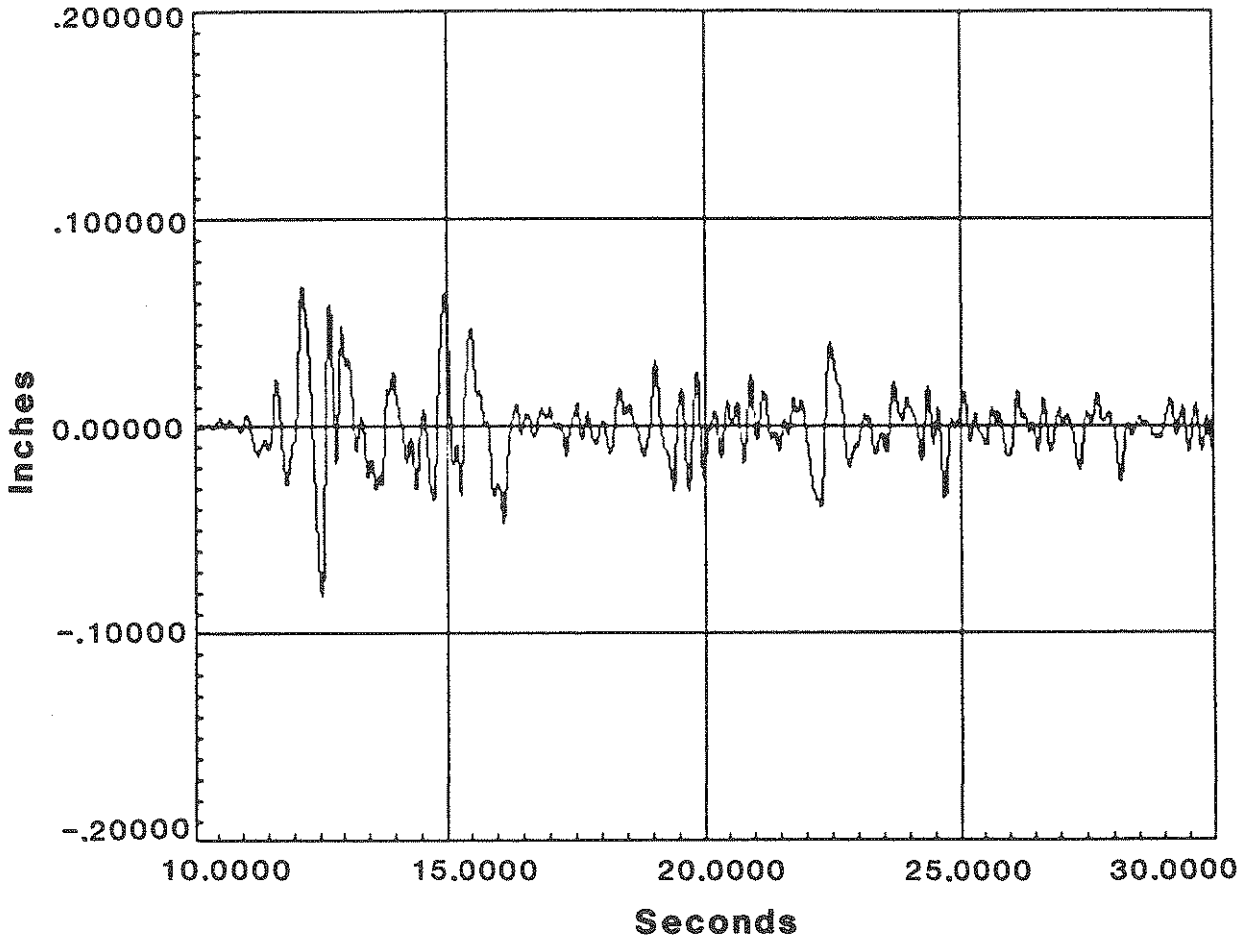

FIGURE 4-20 Relative Displacement Response In Time Domain For Global Closed-Loop Control With β = 1.0 For Seismic Excitation

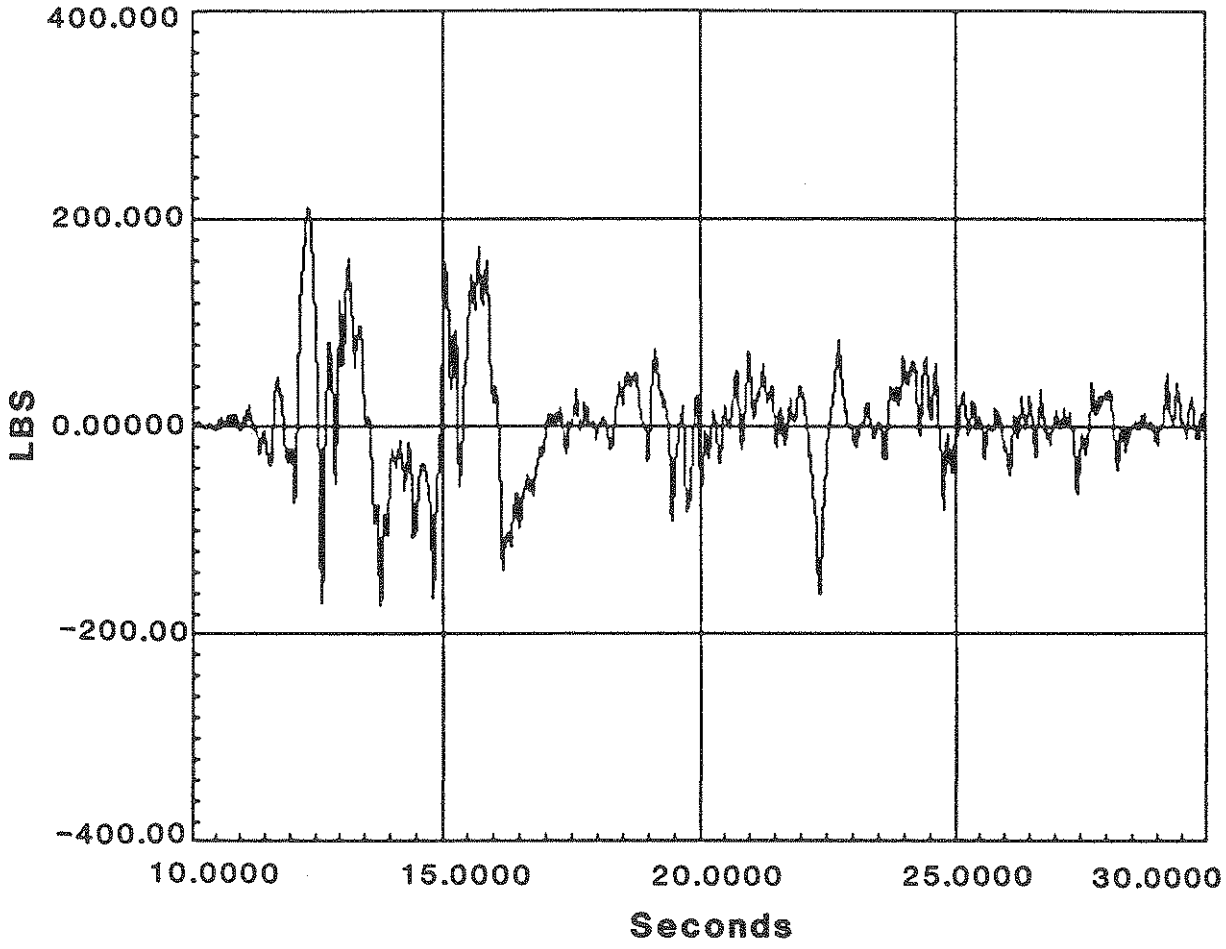

FIGURE 4-21 Time History Of Control Forces For Instantaneous Open-Loop Control With $Q/R = 2 \times 10^6$ For Seismic Excitation

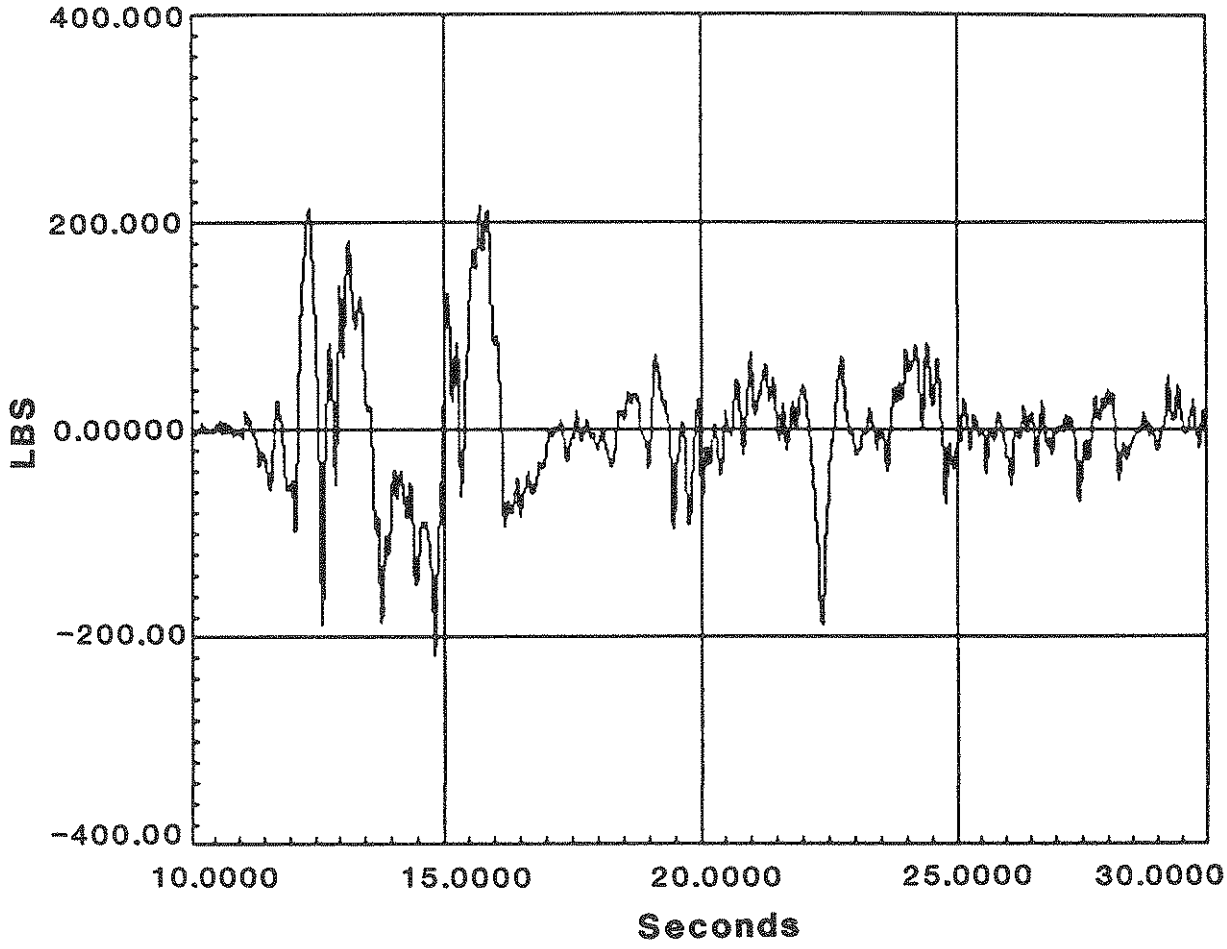

FIGURE 4-22 Time History Of Control Forces For Instantaneous Open-Closed-Loop Control With $Q/R = 2.65 \times 10^6$ For Seismic Excitation

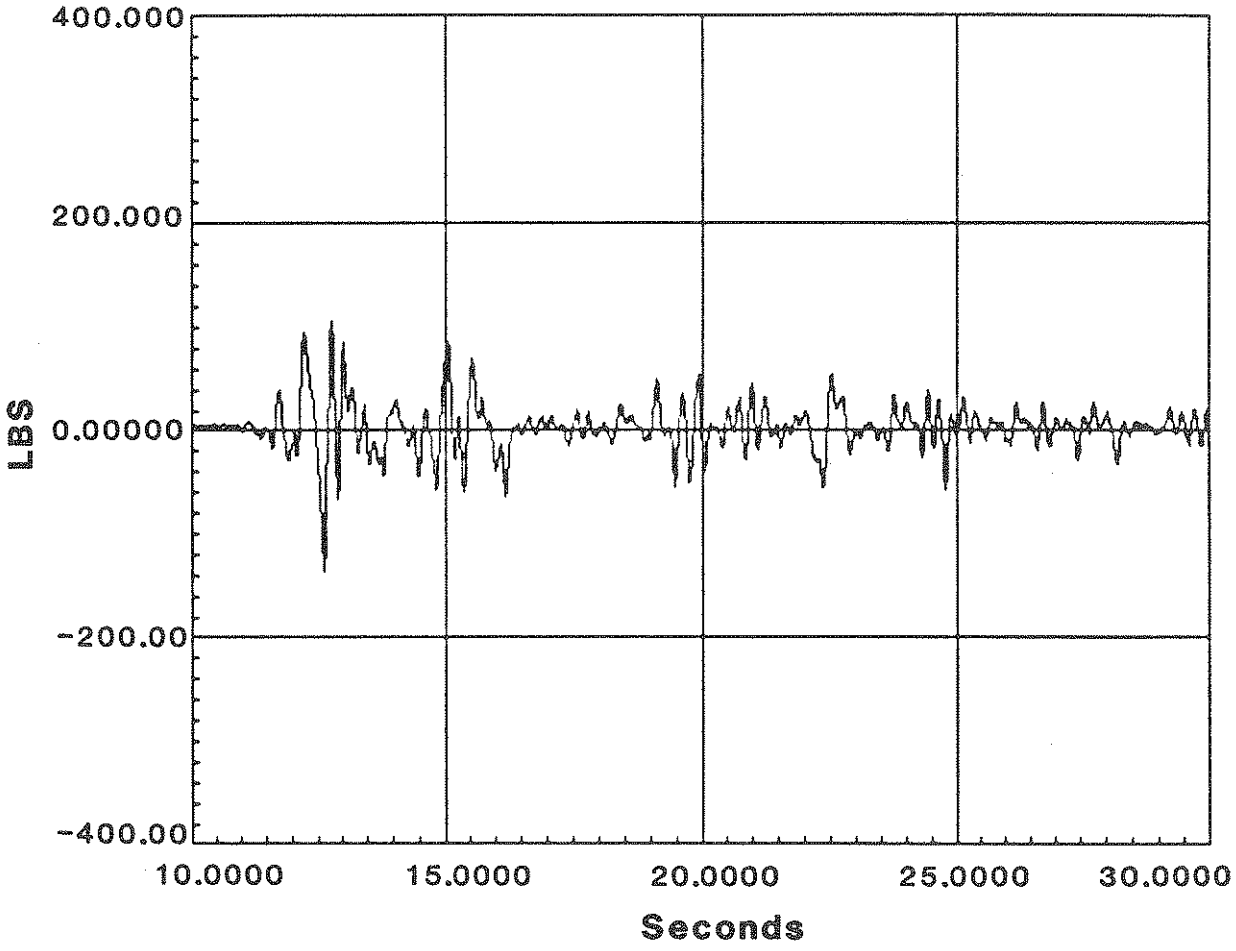

FIGURE 4-23 Time History Of Control Forces For Instantaneous Closed-Loop Control With $Q/R = 2.65 \times 10^6$ For Seismic Excitation

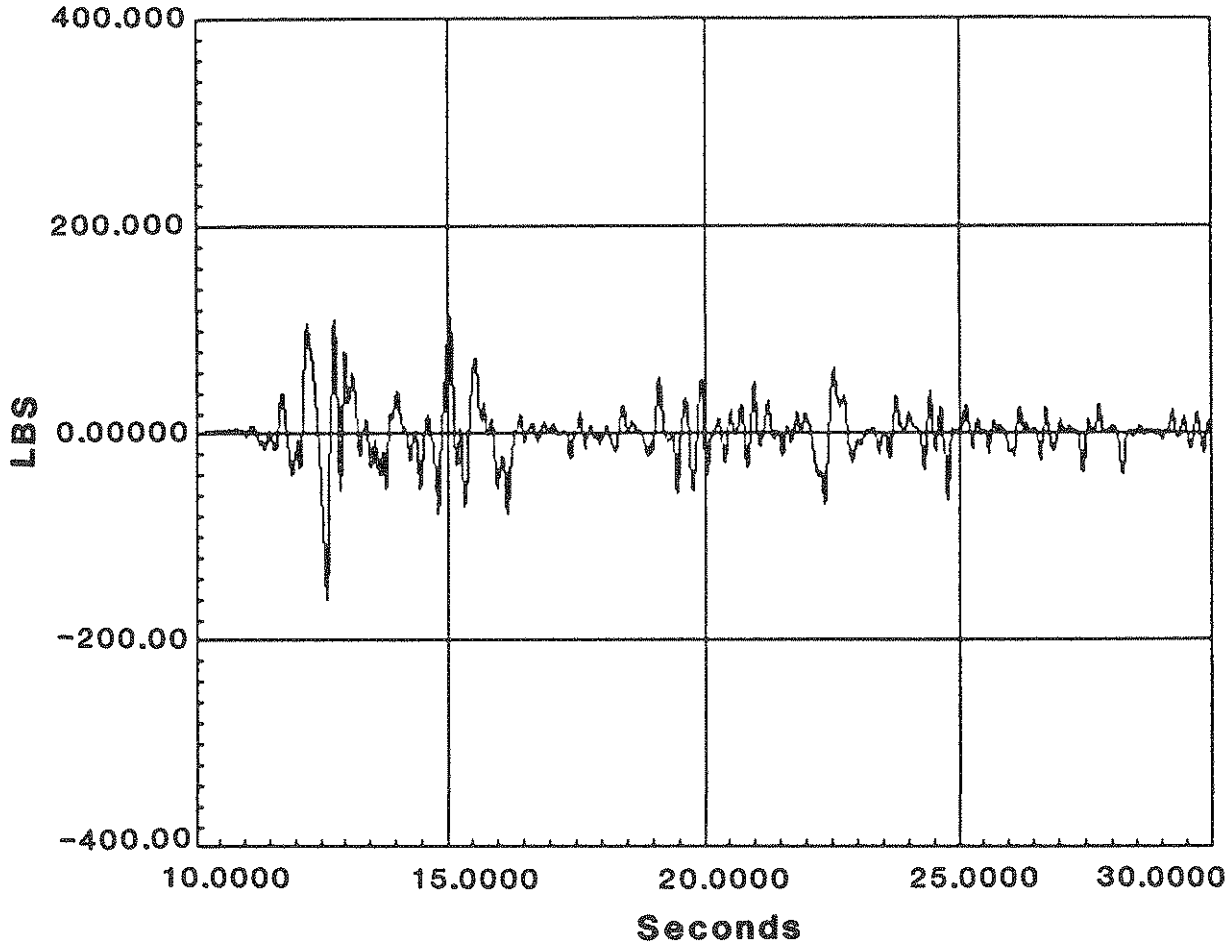

FIGURE 4-24 Time History Of Control Forces For Global Closed-Loop Control With β = 1.0 For Seismic Excitation

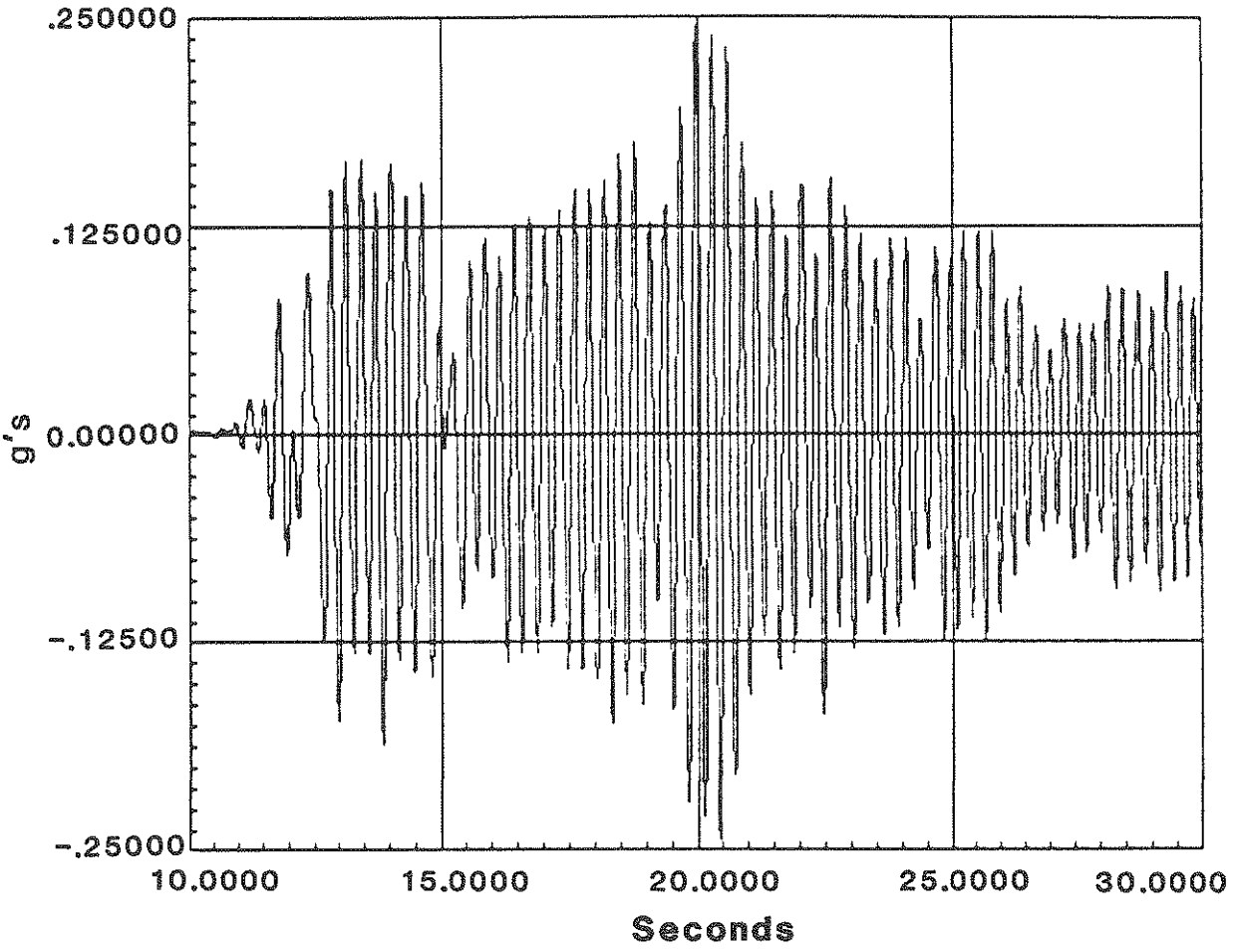

FIGURE 4-25 Time History Of Uncontrolled Absolute Acceleration For Seismic Excitation

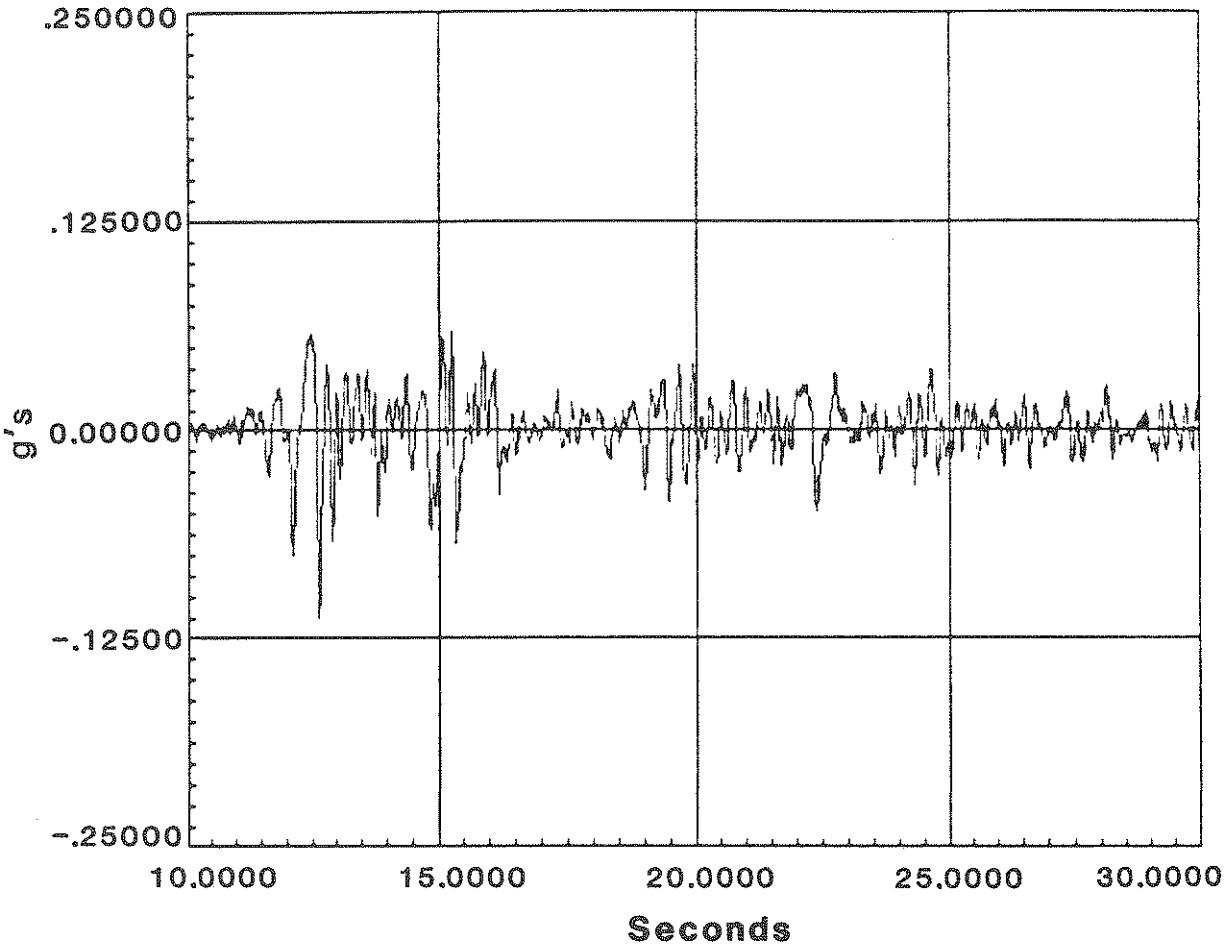

FIGURE 4-26 Time History Of Controlled Absolute Acceleration For Instantaneous Open-Closed-Loop Control With $Q/R = 2.65 \times 10^6$ For Seismic Excitation

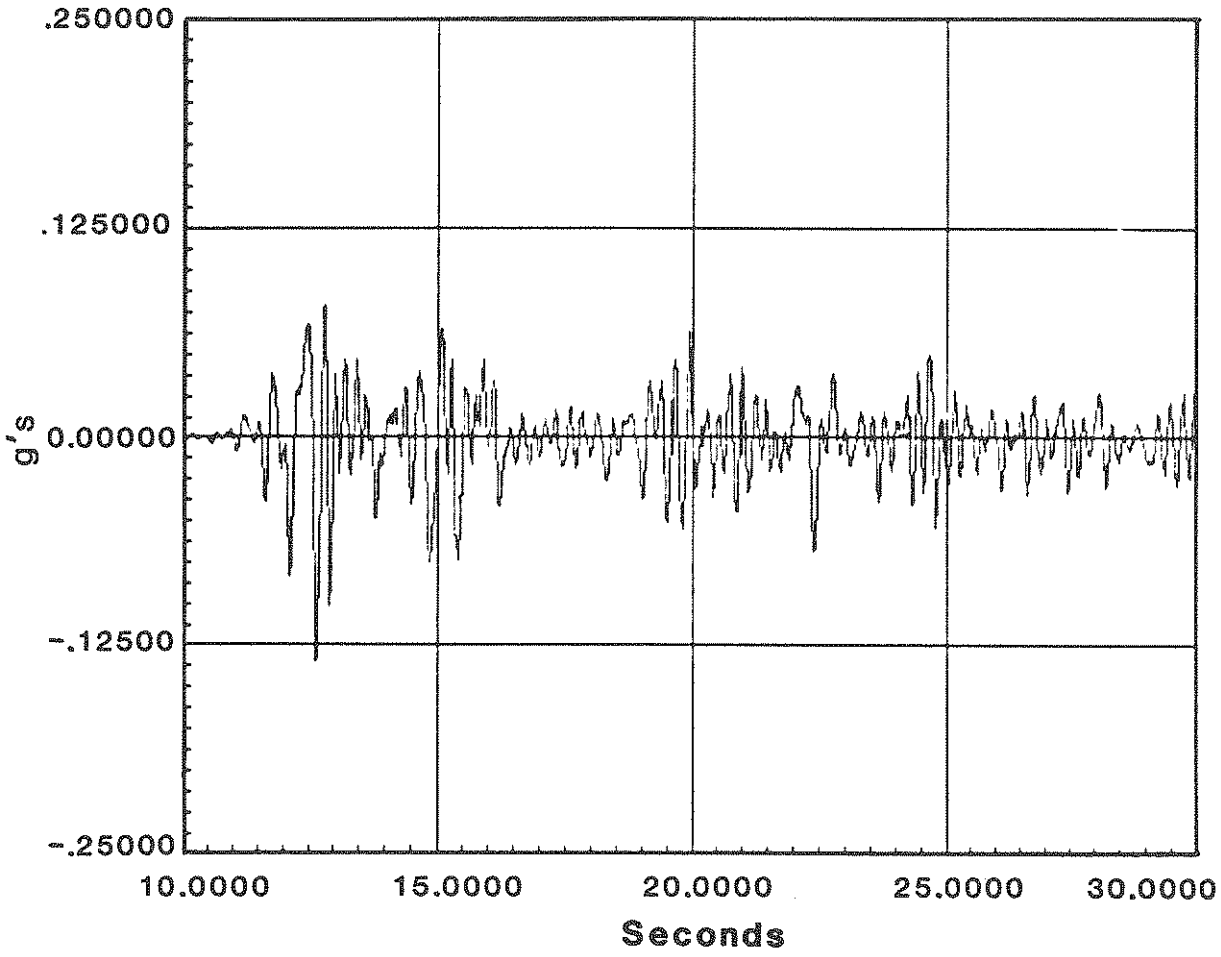

FIGURE 4-27 Time History Of Controlled Absolute Acceleration For Instantaneous Closed-Loop Control With Q/R = 2.65 x 10^6 For Seismic Excitation

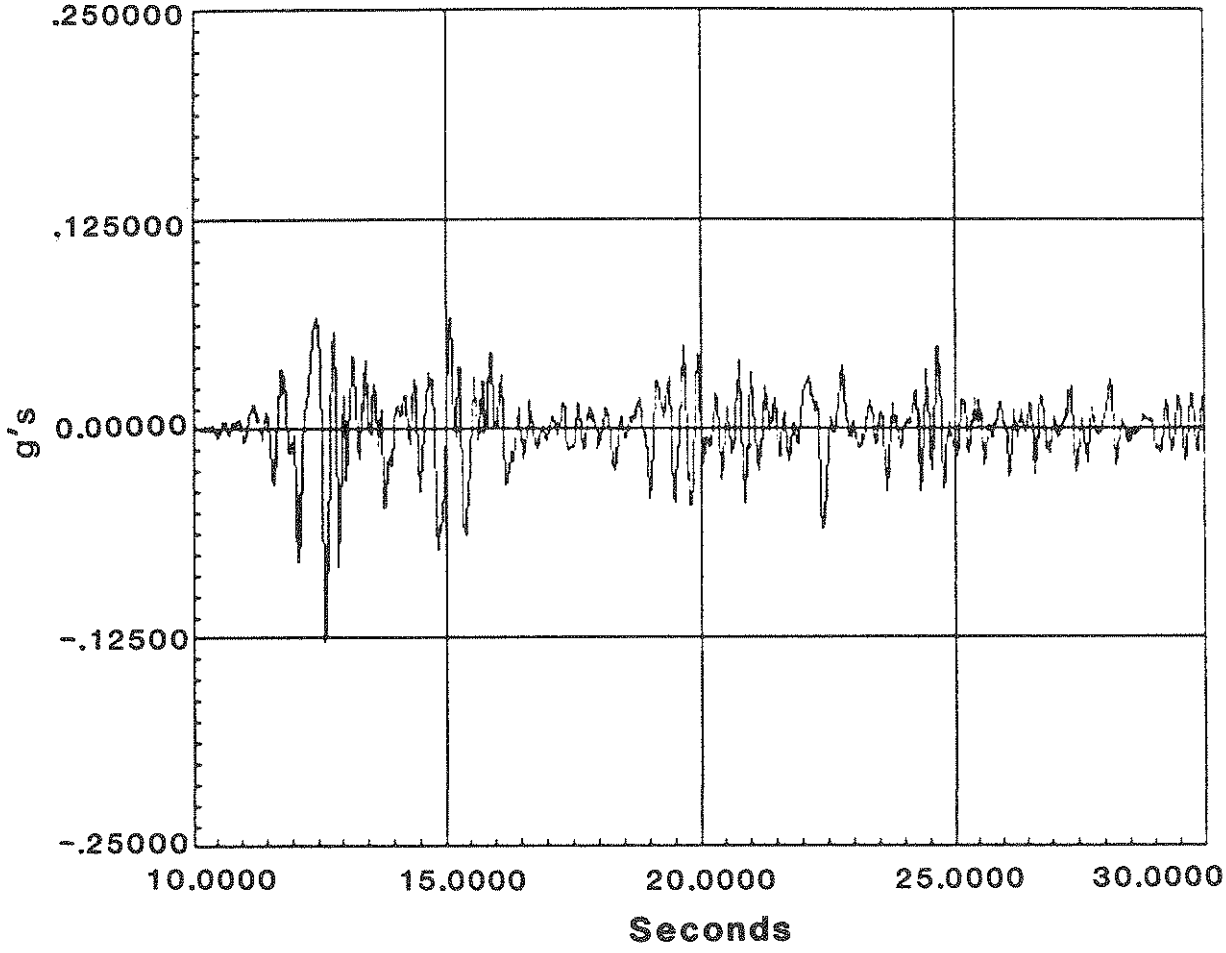

FIGURE 4-28 Time History Of Controlled Absolute Acceleration For Global Closed-Loop Control With β = 1.0 For Seismic Excitation

SECTION 5
CONCLUSION

Based on experimental results, the instantaneous optimal control laws have been shown to be feasible for active structural control under various excitations including seismic excitations. The exception is instantaneous optimal open-loop control where measurement of state variables was necessary to insure its success.

Comparisons between the different control algorithms under instantaneous optimal control law indicated that the closed-loop control performs the best. In the open-loop control and open-closed-loop control, since the base acceleration was considered as a feedback variable in the control algorithms and since time delay compensation was difficult to implement, errors were introduced to the control process, resulting in a degradation of control efficiency.

The instantaneous optimal control algorithms were compared with classical optimal control, and these results are very close to each other if the control parameters are suitably chosen. Since the instantaneous optimal control does not require solving the Riccati matrix equation as required in classical optimal control, computational advantages exist in the use of instantaneous optimal control. This is particularly evident when the number of degree of freedom of the structure under control is large.

SECTION 6
REFERENCES

1. L.L. Chung, A.M. Reinhorn and T.T. Soong, "An Experimental Study of Active Structural Control", **Proc. ASCE Specialty Conference on Structual Dynamics**, Los Angeles, CA, 1986, pp. 795-802.
2. J.N. Yang, A. Akbarpour and P. Ghaemmaghami "Instantaneous Optimal Control Algorithms for Tall Buildings", National Center for Earthquake Engineering Research, Technical Report No. NCEER-87-0007.
3. L.L. Chung, "An Experimental Study of Active Structural Control", M.S. Thesis, State University of New York at Buffalo, Buffalo, NY, December 1985.
4. T.T. Soong, A.M. Reinhorn and J.N. Yang, "A Standardized Model for Structural Control Experiments and Some Experimental Results", **Proc. Second International Symposium on Structure Control**, Waterloo, Canada, 1985, to appear.

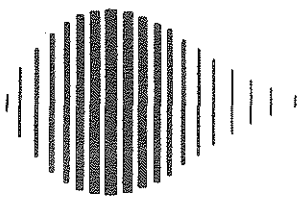

National Center for Earthquake Engineering Research
State University of New York at Buffalo